framatome

Evaluation of Advanced Cladding and Structural Material (M5) in PWR Reactor Fuel

BAW-10227NP
Revision 2

Topical Report

December 2019

Nature of Changes

Item	Section(s) or Page(s)	Description and Justification
1	All	Complete rewrite

Contents

Page

1.0 INTRODUCTION 1-1
2.0 SUMMARY 2-1
3.0 APPLICABLE REGULATORY GUIDANCE 3-1
4.0 RANGE OF APPLICABILITY 4-1
5.0 MATERIAL DEFINITION 5-1
5.1 Material Composition 5-1
5.2 Microstructure 5-1
5.3 Manufacturing 5-1
5.4 Surface Finish 5-2
6.0 OPERATING EXPERIENCE 6-1
6.1 $M5_{Framatome}$ Component Global Operating Experience 6-1
6.2 Fuel Rod Performance Code Database 6-1
6.3 Post-Irradiation Examination High Burnup Database 6-2
7.0 PHYSICAL PROPERTIES 7-1
7.1 Melting Point 7-1
7.2 Density 7-2
7.3 Specific Heat Capacity 7-2
7.4 Thermal Expansion 7-3
7.5 Thermal Conductivity 7-5
7.6 Young's Modulus 7-6
7.7 Poisson's Ratio 7-7
7.8 Emissivity 7-7
7.9 Meyer's Hardness 7-8
8.0 MECHANICAL PROPERTIES 8-1
8.1 Tensile Properties of Unirradiated Material 8-1
8.1.1 Uniaxial Loading 8-1
8.1.2 Biaxial Loading 8-3
8.2 Tensile Properties of Irradiated Material 8-4
8.2.1 Uniaxial Loading 8-4

8.2.2 Biaxial Loading 8-5
8.3 Elongation 8-7
9.0 OXIDATION AND HYDROGEN PICKUP DURING NORMAL OPERATION 9-1
9.1 Corrosion Rate 9-1
9.2 Hydrogen Pickup 9-2
9.3 Corrosion and Hydriding Databases 9-4
9.4 Hydride Morphology in Cladding 9-4
9.5 Limits on Oxidation and Hydriding 9-7
10.0 COMPONENT PERFORMANCE 10-1
10.1 Fuel Rod Stress Limits 10-1
10.2 Fuel Rod Buckling 10-3
10.3 Cladding Creep Collapse 10-3
10.4 Transient Cladding Strain 10-4
10.5 Fuel Rod Fatigue 10-4
10.6 Fretting 10-4
11.0 GROWTH AND CREEP 11-1
11.1 Irradiation Induced Free Growth and Creep 11-1
11.2 Fuel Rod Axial Growth 11-2
11.3 Fuel Assembly Growth 11-3
11.4 Fuel Rod Bowing 11-4
12.0 MATERIAL PERFORMANCE IN NON-LOCA 12-1
13.0 MATERIAL PERFORMANCE IN LOCA 13-1
13.1 Swelling and Rupture 13-1
13.1.1 Swelling and Rupture Model Background 13-1
13.1.2 Swelling and Rupture Database Updates 13-2
13.1.3 Description of EDGAR Tests 13-3
13.1.4 Swelling and Rupture Model 13-3
13.2 High Temperature Steam Oxidation 13-10
13.3 Analytical Limits - 10 CFR 50.46 13-12
14.0 SURVEILLANCE 14-1
15.0 UPDATE PROCESS 15-1
15.1 Model Updates 15-1

15.2 Updates to Applicability Ranges 15-2
15.3 NRC Notifications 15-2
16.0 REFERENCES 16-1

List of Tables

Table 3-1: Acceptance Criteria for $M5_{Framatome}$ Cladding and Structural Components 3-2

Table 5-1: Chemical Composition of $M5_{Framatome}$ Alloy 5-3

Table 9-1: Constants for Corrosion of $M5_{Framatome}$ Components 9-8

Table 10-1: Stress Limits for $M5_{Framatome}$ Cladding 10-6

Table 13-1: Slow and Fast Ramp Rate Pre-Rupture Strain Model for $M5_{Framatome}$ Cladding 13-18

Table 13-2: Slow and Fast Ramp Rate Rupture Strain Model for $M5_{Framatome}$ Cladding 13-20

Table 13-3: Slow and Fast Ramp Rate Assembly Blockage Model with $M5_{Framatome}$ Cladding 13-22

List of Figures

Figure 5-1: $M5_{Framatome}$ Material Fabrication Process Outline 5-4
Figure 6-1: Burnup Distribution of Fuel Assemblies Containing $M5_{Framatome}$ Cladding (through December 2017) 6-3
Figure 6-2: Burnup Distribution of $M5_{Framatome}$ Cladding in the GALILEO Database 6-4
Figure 6-3: $M5_{Framatome}$ Fuel Rod Axial Growth Operating Experience as a Function of Burnup for AFA, GAIA, and HTP Fuel Assemblies 6-5
Figure 6-4: $M5_{Framatome}$ Cladding Corrosion Database used for Validation of GALILEO Fuel Rod Performance Code 6-6
Figure 8-1: Design Uniaxial Yield Strength of Unirradiated $M5_{Framatome}$ Material as a Function of Temperature 8-8
Figure 8-2: Design Uniaxial Tensile Strength of Unirradiated $M5_{Framatome}$ Material as a Function of Temperature 8-9
Figure 8-3: Design Biaxial Yield Strength of Unirradiated $M5_{Framatome}$ Material as a Function of Temperature 8-10
Figure 8-4: Best-Estimate Biaxial Tensile Strength of Unirradiated $M5_{Framatome}$ Material as a Function of Temperature 8-11
Figure 8-5: Best-Estimate Uniaxial Yield strength of Irradiated $M5_{Framatome}$ Material as a Function of Fast Fluence 8-12
Figure 8-6: Best-Estimate Uniaxial Tensile Strength of Irradiated $M5_{Framatome}$ Material as a Function of Fast Fluence 8-13
Figure 8-7: Best-Estimate Biaxial Yield Strength of Irradiated $M5_{Framatome}$ Material as a Function of Fast Fluence 8-14
Figure 8-8: Best-Estimate Biaxial Tensile Strength of Irradiated $M5_{Framatome}$ Cladding as a Function of Fast Fluence 8-15
Figure 9-1: $M5_{Framatome}$ Cladding Hydrogen Content vs. Fuel Burnup (through December 2017) 9-9
Figure 9-2: Measured and Predicted Hydrogen Concentration for $M5_{Framatome}$ Cladding 9-10
Figure 9-3: Post-Transition Hydrogen Pickup Fraction as a Function of Average Oxidation Rate 9-11
Figure 9-4: Comparison of Measured and Predicted Oxide Thickness for Guide Tubes 9-12
Figure 9-5: Comparison of Measured and Predicted Hydrogen Concentration for Guide Tubes 9-13

Figure 9-6: Comparison of Measured and Predicted Oxide Thickness for Spacer Grids 9-14

Figure 9-7: Comparison of Measured and Predicted Hydrogen Concentration for Spacer Grids 9-15

Figure 9-8: Cladding Hydride Morphology in High Burnup Assembly at Elevations of 645 mm (top) and 2847 mm (bottom) 9-16

Figure 11-1: Predicted Fuel Rod Axial Growth by the Upper Bound Model as a Function of Experimental Axial Growth from AFA, GAIA, and HTP Fuel Assemblies 11-5

Figure 11-2: Fuel Rod Axial Growth Operating Experience as a Function of Fuel Rod Average Burnup for GAIA and HTP Fuel Assemblies Compared to the Fuel Rod Axial Growth Upper Bound (UB) Model 11-6

Figure 11-3: $M5_{Framatome}$ HTP Fuel Assembly Growth 11-7

Figure 13-1: EDGAR Test Apparatus 13-24

Figure 13-2: Ruptured Cladding Sample Schematic 13-25

Figure 13-3: Slow and Fast Heating Ramp Rate Pre-Rupture Strain Curves for $M5_{Framatome}$ Cladding 13-26

Figure 13-4: Fast Heating Ramp Rate Rupture Strain Curves and EDGAR Rupture Strain Data for $M5_{Framatome}$ Cladding 13-27

Figure 13-5: Slow and Fast Heating Ramp Rate Rupture Strain Curves for $M5_{Framatome}$ Cladding 13-28

Figure 13-6: Fast Heating Ramp Rate Assembly Blockage Curves with $M5_{Framatome}$ Cladding 13-29

Figure 13-7: Slow and Fast Heating Ramp Rate Assembly Blockage Curves with $M5_{Framatome}$ Cladding 13-30

Figure 13-8: Measured and Calculated % ECR at 1200 °C 13-31

Figure 13-9: Measured and Calculated % ECR at 1000 °C 13-32

Figure 13-10: Measured and Calculated % ECR at 1100 °C 13-33

Figure 13-11: Measured and Calculated % ECR at 1250 °C 13-34

Figure 13-12: Qualitative Diagram of Oxygen Concentration in Zircaloy Cladding Exposed at High Temperature to Steam on the Outside Surface and Cooled to Room Temperature 13-35

Figure 13-13: RCT Residual Ductility vs. Calculated ECR, 1200 °C Oxidation 13-36

Figure 13-14: RCT Residual Ductility vs. Calculated ECR, 1000 °C -1250 °C Oxidation 13-37

Nomenclature

Acronym	Definition
AOO	Anticipated Operational Occurrence
ASME	American Society of Mechanical Engineers
B&W	Babcock and Wilcox
BJ	Baker-Just
BOL	Beginning of Life
BU	Burnup
CE	Combustion Engineering
CEA	Commissariat à l'Energie Atomique
CFR	Code of Federal Regulations
CP	Cathcart-Pawel
DBT	Ductile-to-brittle transition
DNB	Departure from Nucleate Boiling
ECCS	Emergency Core Cooling System
ECR	Equivalent cladding reacted
EOL	End of life
GWd	Gigawatt days
LOCA	Loss Of Coolant Accident
mtU	Metric Ton of Uranium
MLO	Maximum Local Oxidation
NRC	U.S. Nuclear Regulatory Commission
PCMI	Pellet-Cladding Mechanical Interaction
PCT	Peak Cladding Temperature
PIE	Post-Irradiation Examination
ppm	parts per million (by weight)
PWR	Pressurized Water Reactor
RAI	Request for Additional Information
RCT	Ring compression test
RG	Regulatory Guide
RLBLOCA	Realistic Large Break Loss Of Coolant Accident
SAFDL	Specified Acceptable Fuel Design Limit
SRP	Standard Review Plan
W	Westinghouse
Zr-4	Zircaloy-4

ABSTRACT

The purpose of this topical report is to present the definition and characteristics for $M5_{Framatome}$ material as an advanced cladding and structural material for use in pressurized water reactor (PWR) fuel assemblies. This report provides updates to the $M5_{Framatome}$ material characteristics based on data collected since the approval of BAW-10227P-A Revision 1 (Reference [1]). The iron content of $M5_{Framatome}$ material was previously updated in Reference [2]. NRC approval for $M5_{Framatome}$ material as a fuel rod cladding material is requested to [

] The $M5_{Framatome}$ material is a proprietary variant of Zr - 1 wt. % Nb.

A discussion is presented of the current regulatory guidance related to cladding as well as structural material. This guidance is found primarily in NUREG-0800 Section 4.2 (Reference [3]). A comparison of applicable NUREG-0800 Section 4.2 criteria and the design evaluation input for the $M5_{Framatome}$ material is provided.

The composition of $M5_{Framatome}$ material is defined. The $M5_{Framatome}$ microstructure and manufacturing process is described. The irradiation experience with $M5_{Framatome}$ material to-date is summarized. Fuel assemblies with $M5_{Framatome}$ cladding, guide tubes, instrument tubes, and spacer grids have been irradiated and provide information about the material behavior.

The physical properties, mechanical behavior, oxidation and hydrogen pick-up fractions, irradiation growth and creep are defined. The application of these properties to design evaluations is summarized and the impact on component performance is discussed. An updated model for fuel rod growth is provided, and the fuel assembly growth correlation is confirmed. [

]

The plans for surveillance of the $M5_{Framatome}$ material behavior are presented. An update process is defined for the property and performance models and applicability ranges for $M5_{Framatome}$ cladding used as input to the design evaluations. This update process involves notification to the NRC under defined conditions.

1.0 INTRODUCTION

The purpose of this topical report is to present the definition and characteristics for $M5_{Framatome}$ (also referred to as M5) material as an advanced cladding and structural material for use in PWR fuel assemblies. $M5_{Framatome}$ material is a proprietary variant of Zr - 1 wt. % Nb. This report provides updates to the material characteristics based on data collected since the approval of BAW-10227P-A Revision 1 (Reference [1]),

[

] The iron content was previously updated in Reference [2]. This revision does not invalidate models approved in previous revisions for application in various methods except as identified in Section 13.1.2.

NRC approval for $M5_{Framatome}$ material as a fuel rod cladding material is requested [

]

Section 3.0 discusses the regulatory requirements of the Standard Review Plan, and Section 4.0 defines the requested range of applicability. Section 5.0 provides a definition of $M5_{Framatome}$ material including its composition and microstructural state. Framatome's operating experience with $M5_{Framatome}$ components is described in Section 6.0. The physical and mechanical properties are provided in Sections 7.0 and 8.0, respectively. Section 9.0 presents the oxidation and hydrogen pickup models. Section 10.0 discusses various aspects of performance that are relevant to fuel system damage and fuel rod failure. Creep and free growth are discussed in Section 11.0. Material performance in non-LOCA accidents is discussed in Section 12.0 and the material performance in LOCA is presented in Section 13.0. Framatome's planned ongoing surveillance is covered in Section 14.0. Future data may require updates to models in this report. Section 15.0 describes a process for updating the report.

2.0 SUMMARY

This topical report describes operating experience, reactor performance, and models needed to design and analyze $M5_{Framatome}$ cladding and structural components. An update process is defined that facilitates Framatome's ability to monitor future performance of $M5_{Framatome}$ material and to update the models as necessary.

The following approach is used to demonstrate that $M5_{Framatome}$ material is suitable for use in fuel assemblies:

- The Standard Review Plan (Reference [3]) is reviewed to determine the criteria that apply to cladding, guide tubes, instrument tubes, and spacer grids.
- A definition of $M5_{Framatome}$ material is provided, in terms of both composition and manufacturing processes. The definition provides confidence that the material will retain its distinctive characteristics and that future performance will be consistent with the available experience.
- The materials-related input for design evaluations of these components is identified. Some of the input, such as density and the coefficients of thermal expansion, are used directly in analytical models. Values or equations for the input, based on laboratory measurements, are provided. Other input, such as corrosion rate and fuel assembly growth, can only be determined by irradiation tests. Empirical correlations based on irradiation experience are provided. All of the materials-related input needed to show compliance with the Standard Review Plan is discussed.
- Performance under Loss of Cooling Accident (LOCA) conditions is discussed, including a concise summary of the swelling and rupture model, high temperature oxidation, and applicability of the 10 CFR 50.46 criteria. [

]

- Irradiation experience and surveillance plans are summarized. Experience provides assurance that the material performs consistently in a variety of fuel assembly designs. Surveillance ensures that any changes in performance will be promptly detected, and if necessary, appropriate actions can be taken.
- Content from Reference [2] is incorporated, which demonstrated that extending the maximum allowable iron concentration does not significantly impact performance.

$M5_{Framatome}$ components have been irradiated in over 100 reactors worldwide and fuel rods utilizing $M5_{Framatome}$ cladding have [

] demonstrating extensive industrial experience. Component performance has been measured through post-irradiation examinations (PIE) and continues to show consistent, predictable behavior.

The material-specific input and models necessary to support Framatome's NRC-approved methodologies for $M5_{Framatome}$ material are presented in this report.

3.0 APPLICABLE REGULATORY GUIDANCE

A review of NUREG-0800 Section 4.2 (Reference [3]) guidance relevant to cladding and structural components is provided in Table 3-1. The table includes acceptance criteria from Reference [3] which are applicable to cladding, guide tubes, instrument tubes, and spacer grids. For those acceptance criteria that are applicable, models are needed to support evaluation of the criteria. The section in this topical report where the model is addressed is indicated.

Table 3-1: Acceptance Criteria for $M5_{Framatome}$ Cladding and Structural Components

NUREG-0800 Section 4.2 Acceptance Criteria	Topical Report Section(s)
1.A. Fuel System Damage	
1.A.i Stress, strain, or loading limits	Fuel rod stress intensity limits are discussed in Section 10.1.
1.A.ii Cumulative strain fatigue cycles	Material fatigue performance is covered in Section 10.5.
1.A.iii Fretting wear	Fretting behavior is addressed in Section 10.6.
1.A.iv Oxidation, hydriding, and crud	Oxidation and hydrogen pickup of components is addressed in Section 9.0.
1.A.v Dimensional changes	Irradiation-induced dimensional changes are discussed in Sections 11.0 - 11.4.
1.A.vi Internal Rod Pressure	This requirement is not addressed by this topical report.
1.A.vii Assembly Liftoff	This requirement is not addressed by this topical report.
1.A.viii Control rod reactivity and insertability	This requirement is not addressed by this topical report.
1.B. Fuel Rod Failure	
1.B.i Hydriding	Internal sources of hydrogen are controlled during manufacturing by product specifications that limit the moisture content. No additional analyses are performed for internal hydriding. External hydriding is discussed in Section 9.0.

NUREG-0800 Section 4.2 Acceptance Criteria	Topical Report Section(s)
1.B.ii Cladding Collapse	Fuel rod buckling and cladding creep collapse are addressed in Sections 10.1 and 10.2, respectively.
1.B.iii Overheating of Cladding	This requirement is not addressed by this topical report.
1.B.iv Overheating of Fuel Pellets	This requirement is not addressed by this topical report.
1.B.v Excessive Fuel Enthalpy	This requirement is not addressed by this topical report.
1.B.vi Pellet/Cladding Interaction	The transient cladding strain limit is confirmed in Section 10.4.
1.B.vii Bursting	Swelling and rupture models are discussed in Section 13.1.
1.B.viii Mechanical Fracturing	Fuel rod stress intensity limits under faulted conditions are provided in Section 10.1.
1.C. Fuel Coolability	
1.C.i Cladding Embrittlement	Analytical limits associated with 10 CFR 50.46(b) are addressed in Section 13.3.
1.C.ii Violent Expulsion of Fuel	This requirement is not addressed by this topical report.
1.C.iii Generalized Cladding Melting	This requirement is not addressed by this topical report.
1.C.iv Fuel Rod Ballooning	Ballooning is addressed in the swelling and rupture discussion in Section 13.1.
1.C.v Structural Deformation	LOCA Post-quench ductility and the 10 CFR 50.46 temperature and oxidation limits are addressed in Section 13.3. Fuel rod stress intensity limits for Safe Shutdown Earthquake are covered in Section 10.1.

4.0 RANGE OF APPLICABILITY

$M5_{Framatome}$ material is an advanced cladding and structural material used in pressurized water reactor fuel. Material properties and performance models are updated in this revision, based on the expanded test database since the approval of BAW-10227P-A Revision 1 (Reference [1]). $M5_{Framatome}$ material limits are [

] This revision is consistent with the $M5_{Framatome}$ cladding models applied in Framatome's advanced fuel rod performance code (Reference [4]).

The updated models in this revision are intended for [

] The range of applicability is addressed with each model. This revision does not invalidate models approved in previous revisions for application in various methods except as identified in Section 13.1.4.

5.0 MATERIAL DEFINITION

$M5_{Framatome}$ material is a proprietary variant of the Zr - 1 wt. % Nb alloy. It is only used in the fully recrystallized annealed condition for cladding as well as structural components. Compared to Zircaloy-4 material, $M5_{Framatome}$ material shows improved corrosion behavior, hydrogen pickup, and growth due to in-core operation.

5.1 *Material Composition*

The chemical composition of $M5_{Framatome}$ material is provided in Table 5-1. Additional composition limits, including the modified composition limits approved in Reference [2], are defined in the manufacturing material specifications and controlled by the manufacturing processes.

5.2 *Microstructure*

$M5_{Framatome}$ material has a fully recrystallized annealed structure [

]

5.3 *Manufacturing*

The manufacturing process for $M5_{Framatome}$ products (cladding tubes, guide tubes, instrument tubes, and spacer grids from sheet material) has been optimized to produce a fully recrystallized and thermodynamically stable microstructure.

The thermomechanical processing steps for the production of tubing and sheet are shown in Figure 5-1.

5.4 *Surface Finish*

The surface finish defined by the manufacturing drawings or specifications is used as the limiting criterion for design purposes. Measurements of the actual surface finish of $M5_{Framatome}$ cladding are similar to those for Zircaloy-4 cladding (Section A.2.1.3 of Reference [1]).

Table 5-1: Chemical Composition of $M5_{Framatome}$ Alloy

[
]

Figure 5-1: $M5_{Framatome}$ Material Fabrication Process Outline

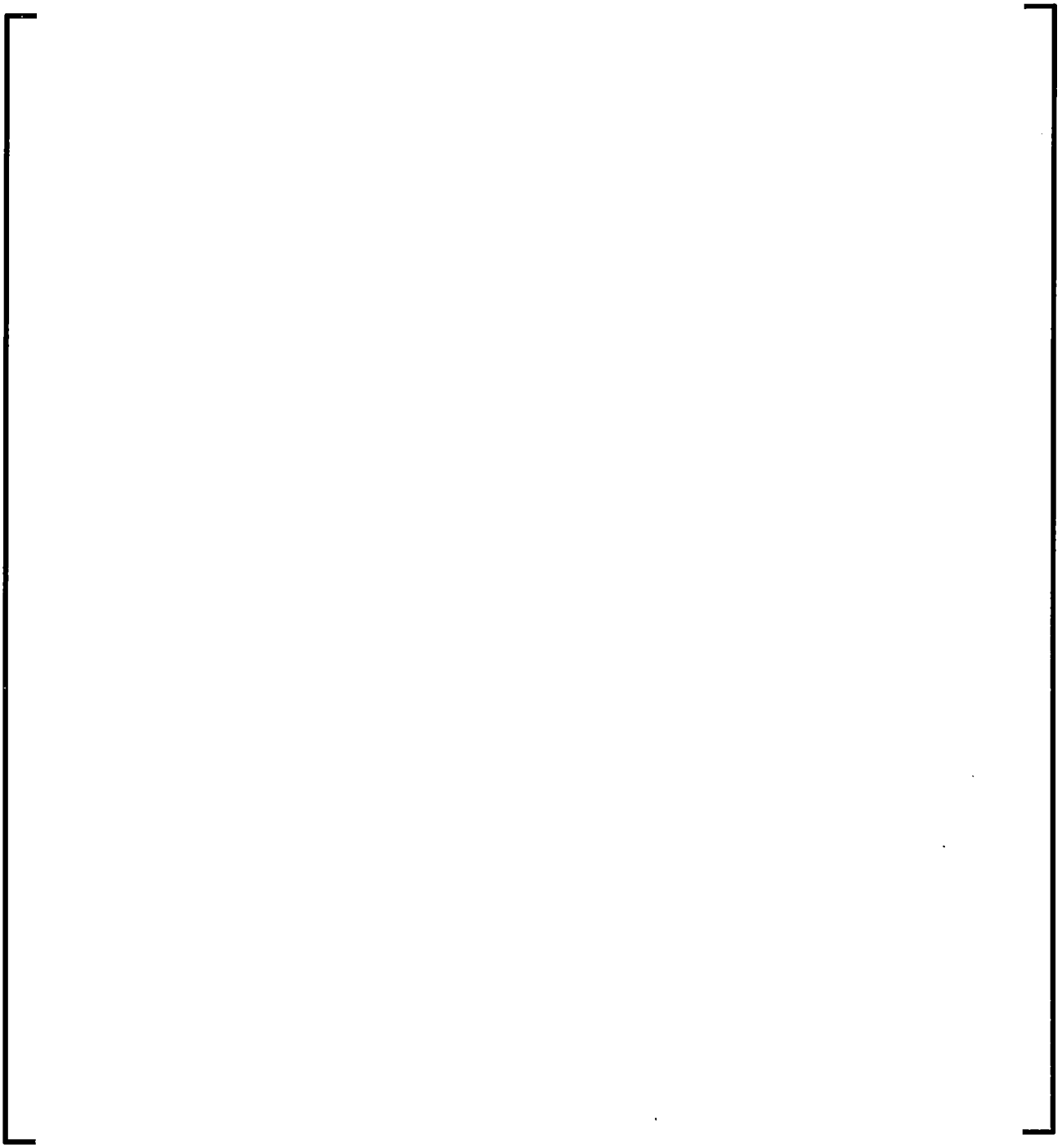

6.0 OPERATING EXPERIENCE

6.1 *$M5_{Framatome}$ Component Global Operating Experience*

Since 1993, over six million fuel rods with $M5_{Framatome}$ cladding have operated in over 100 commercial reactors globally. Fuel rods with $M5_{Framatome}$ cladding have operated in fuel assembly arrays including 14×14, 15×15, 16×16, 17×17, and 18×18 and in all modern Framatome fuel assembly designs. The fuel assembly average burnups achieved for the [ ] irradiated fuel assemblies containing $M5_{Framatome}$ cladding are shown in Figure 6-1. This operating experience includes [ ] fuel assemblies containing $M5_{Framatome}$ spacer grids and guide tubes (with a maximum fuel assembly burnup reached of [ ]) and [ ] fuel assemblies containing $M5_{Framatome}$ guide tubes and Zircaloy-4 spacer grids (with a maximum fuel assembly burnup reached of [ ]) as of December 2017.

6.2 *Fuel Rod Performance Code Database*

The models applied in fuel rod performance codes are based on a database of fuel rod performance results obtained from a defined subset of fuel rods. For example, the overall GALILEO database (Reference [4]) includes $M5_{Framatome}$ cladding irradiated [ ] The rod average burnup distribution for $M5_{Framatome}$ cladding included in the GALILEO fission gas release database is shown in Figure 6-2. [ ] of the $M5_{Framatome}$ cladding in the GALILEO fission gas release database reached [ ]

6.3 *Post-Irradiation Examination High Burnup Database*

Fuel rods are periodically examined to measure fuel rod growth and $M5_{Framatome}$ cladding corrosion following irradiation in commercial reactors. Databases containing these measurements have been used to develop models that predict cladding behavior [ ] The fuel rod growth measurement database is extensive and is described in Section 11.2 and shown in Figure 6-3. This database incorporates $M5_{Framatome}$ cladding irradiated in modern Framatome fuel assembly design types, including various fuel rod designs, pellet types, and dimensions. The fuel rod growth database used to develop the fuel rod growth model represents $M5_{Framatome}$ cladding irradiation in 30 reactors worldwide, including array types of 14×14, 15×15, 16×16, 17×17, and 18×18. It incorporates growth impacts from differing fuel rod designs, pellet designs, and reactor operating conditions. The fuel rod growth database includes growth measurements [

]

The global database of $M5_{Framatome}$ cladding corrosion measurements is vast, incorporating over [ ] measurements. An excerpt of the data used in validation of $M5_{Framatome}$ cladding corrosion models implemented in GALILEO code (Reference [4]) is shown in Figure 6-4. This subset of data includes measurements from over [ ] fuel rods collected at poolside and in hot cells using either eddy current techniques or metallography. The $M5_{Framatome}$ cladding corrosion database used in GALILEO code includes measurements [

]

Figure 6-1: Burnup Distribution of Fuel Assemblies Containing $M5_{Framatome}$ Cladding (through December 2017)

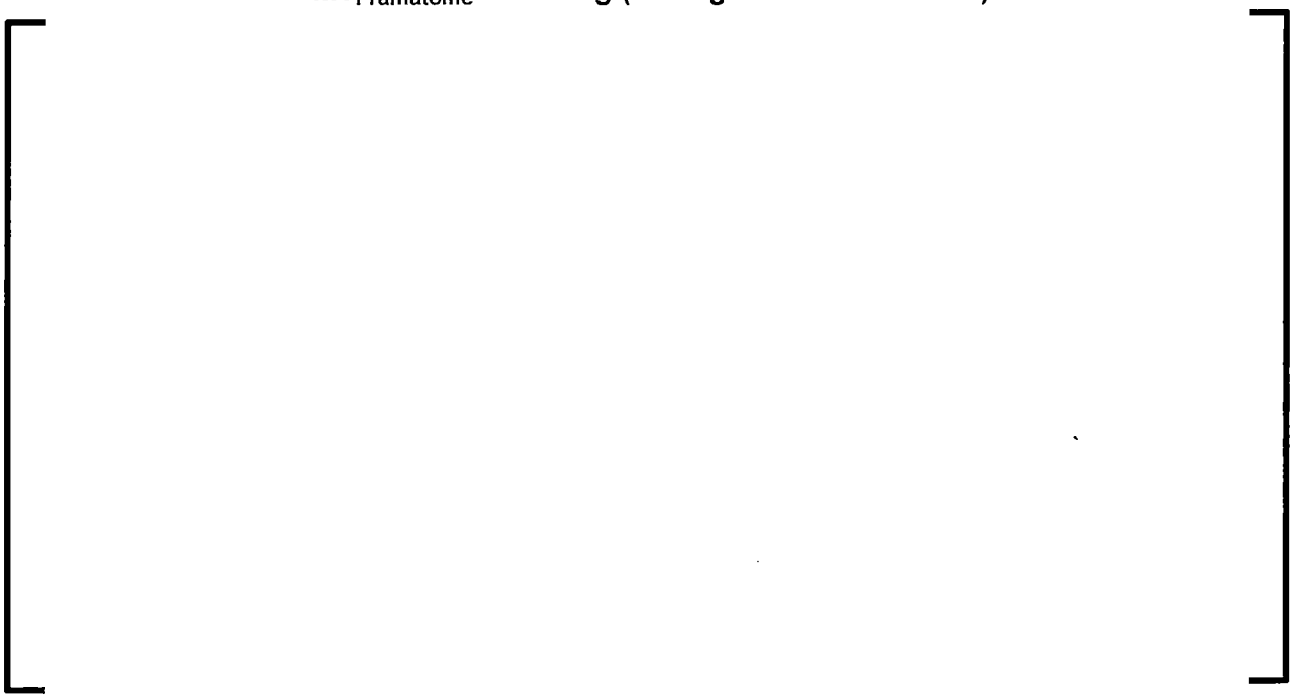

Figure 6-2: Burnup Distribution of $M5_{Framatome}$ Cladding in the GALILEO Database

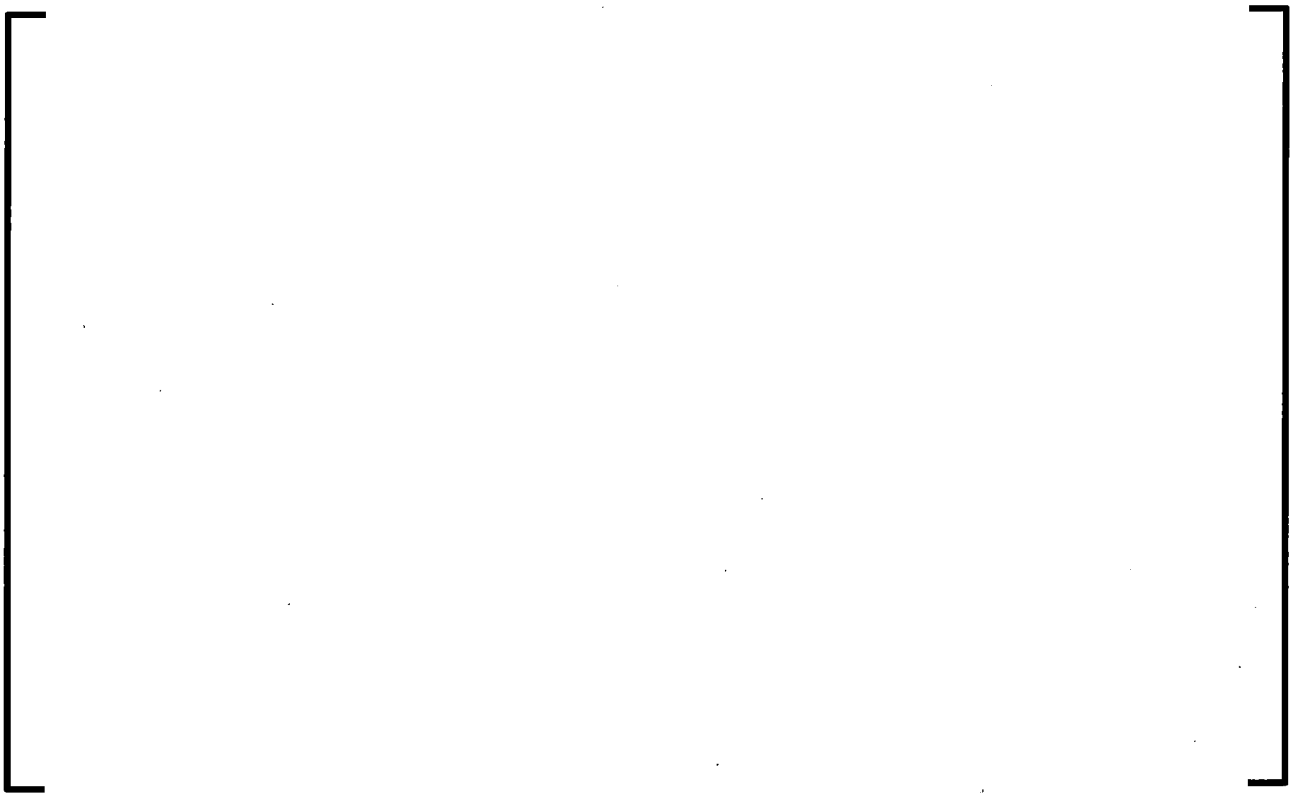

Figure 6-3: $M5_{Framatome}$ Fuel Rod Axial Growth Operating Experience as a Function of Burnup for AFA, GAIA, and HTP Fuel Assemblies

Figure 6-4: $M5_{Framatome}$ Cladding Corrosion Database used for Validation of GALILEO Fuel Rod Performance Code

7.0 PHYSICAL PROPERTIES

This section provides values for the physical properties of $M5_{Framatome}$ material. The first five subsections discuss melting point, density, specific heat capacity, thermal expansion, and thermal conductivity. Young's modulus and Poisson's ratio, sometimes classified as mechanical properties, are discussed in the next two subsections. The remaining subsections discuss emissivity and Meyer's hardness. The physical properties are used in various methodologies to perform design analyses of fuel rod and assembly structural components and have been approved up to burnups of 62 GWd/mtU. Their use is justified to [ ]

Models must be appropriate for their application, and therefore differences may exist between models identified herein and those approved for use in other methodologies. Unless found to incorrectly represent the performance of $M5_{Framatome}$ material, models used in other methodologies need not be identical to those in this report.

7.1 *Melting Point*

The alloying elements in $M5_{Framatome}$ material have different effects on the melting (solidus) temperature of zirconium, with oxygen tending to increase the melting point and niobium tending to decrease it. [

]

Melting of structural parts could compromise the coolability of a fuel assembly. However, the temperatures required to melt $M5_{Framatome}$ material are well above those required to embrittle the cladding, so no design analysis of melting is needed (Section II.1.C.iii of Reference [3]).

Because the melting point is high, it is expected that any radiation damage would be annealed at temperatures well below the melting point. The melting point is also a structure-insensitive property (page 86 of Reference [6]), so it will not be significantly affected by irradiation for [ ]

7.2 *Density*

A [ ] is used for $M5_{Framatome}$ material. The density at other temperatures may be calculated by applying the equations for thermal expansion that are provided in Section 7.4.

[

]

[

] Section 2.1 of the Safety Evaluation for BAW-10227P in Reference [1] approved the value for fuel rod average burnups up to 62 GWd/mtU. Density is a structure-insensitive property (page 86 of Reference [6]), so it will not be significantly affected by irradiation [ ]

7.3 *Specific Heat Capacity*

The specific heat capacity of $M5_{Framatome}$ material is represented by the following equations:

[ ]

[

] Section 2.4 of the Safety Evaluation for BAW-10227P in Reference [1] approved the equations above for fuel rod average burnups up to 62 GWd/mtU. Specific heat capacity is a structure-insensitive property (page 86 of Reference [6]), so it will not be significantly affected by irradiation for [

]

7.4 *Thermal Expansion*

$M5_{Framatome}$ material is anisotropic, so separate equations for thermal expansion are provided for the axial, tangential, and radial directions:

[

[

[

] The equations for thermal expansion are applicable to cladding and guide tubes, and the equations for axial expansion also apply to expansion of sheet in the rolling direction.

For a thin-walled tube, the equations for the radial direction determine the change in wall thickness, and the equations for the tangential direction determine the change in diameter. The equations for the axial direction determine changes in length.

Values for the coefficient of thermal expansion in the axial direction are reported to range between 5.2×10^{-6} K^{-1} and 6×10^{-6} K^{-1} for various zirconium alloys including Zircaloy-2, Zircaloy-4, Zr - 2.5 wt. % Nb, and Zr - 1 wt. % Nb. [

]

[

] Sections 3.1.1.7, 3.2.1.7, and 4.0 of the Safety Evaluation for Reference [8] approved the equations above for fuel rod average burnups up to 62 GWd/mtU. The coefficient of thermal expansion is a structure-insensitive property (page 86 of Reference [6]), so it will not be significantly affected by irradiation for [ ]

7.5 *Thermal Conductivity*

The thermal conductivity of $M5_{Framatome}$ cladding and guide tube material is represented as follows:

[

[

] Section 2.3 of the Safety Evaluation for BAW-10227P in Reference [1] approved the equation above for fuel rod average burnups up to 62 GWd/mtU. It is expected that any effect of irradiation will saturate at much lower [ ] so there will not be a significant additional effect of irradiation

[ ]

7.6 *Young's Modulus*

Two models have been developed [

]

[

]

[

]

7.7 *Poisson's Ratio*

Poisson's ratio for $M5_{Framatome}$ material is [ ] That value has been approved for analyses of normal operations and LOCA at fuel rod average burnups up to 62 GWd/mtU (Section 2.11 of the Safety Evaluation for BAW-10227P in Reference [1]; Sections 3.1.1.9, 3.2.1.9, and 4.0 of the Safety Evaluation for Reference [8]). [

] Like Young's modulus, Poisson's ratio is not applicable to plastic deformation. Because elastic strains are small, the value of Poisson's ratio has only a small effect on LOCA calculations. Poisson's ratio is a structure-insensitive property (page 86 of Reference [6]), so it will not be significantly affected by irradiation for [

]

[

]

7.8 *Emissivity*

The emissivity of $M5_{Framatome}$ material is represented by the following equations.

[

]

[ ] (Sections 4.1.10 and 5.1.10 of Reference [8]; Sections 3.1.1.10 and 3.2.1.10 of Safety Evaluation for Reference [8]; and Section 7.9.3.6.5 of Reference [10]). The transition temperature [ ] is that at which the two equations provide the same value.

Sections 3.1.1.10, 3.2.1.10, and 4.0 of the Safety Evaluation for Reference [8] approved the equations above for fuel rod average burnups up to 62 GWd/mtU. Emissivity is a structure-insensitive property (page 95 of Reference [11]), so it is expected that there will not be a significant effect of irradiation for [

]

7.9 *Meyer's Hardness*

Meyer's hardness for $M5_{Framatome}$ material is represented by the following equation:

Section 2.13 of the Safety Evaluation for BAW-10227P in Reference [1] approved the equation above for fuel rod average burnups up to 62 GWd/mtU. It is expected that the effect of irradiation will saturate [ ] so there will not be a significant additional effect of irradiation [

]

8.0 MECHANICAL PROPERTIES

This section provides values for the mechanical properties of $M5_{Framatome}$ material. Young's modulus and Poisson's ratio, sometimes classified as mechanical properties, are discussed in Section 7.6 and 7.7 respectively. The mechanical properties are used in various methodologies to perform design analyses of fuel assembly components.

8.1 *Tensile Properties of Unirradiated Material*

8.1.1 Uniaxial Loading

8.1.1.1 Yield Strength

The design value for the uniaxial yield strength at room temperature is the minimum value allowed by the manufacturing specifications for tubing:

[ ]

[ ] The value is applicable to cladding and guide tubes.

For temperatures from [ ] the design value for uniaxial yield strength is:

[ ]

[ ] The equations are applicable to cladding and guide tubes. The design uniaxial yield strength for unirradiated $M5_{Framatome}$ material is plotted as a function of temperature in Figure 8-1.

8.1.1.2 Tensile Strength

The design value for the uniaxial tensile strength at room temperature is the minimum value allowed by the manufacturing specifications for tubing:

[ ]

[ ] The value is applicable to cladding and guide tubes.

For temperatures from [ ] the design value for uniaxial tensile strength is:

[ ]

[ ] The equations are applicable to cladding and guide tubes.

For temperatures from [ ] the design value for uniaxial tensile strength is [ ]

[

]

The design uniaxial tensile strength for unirradiated $M5_{Framatome}$ material is plotted as a function of temperature in Figure 8-2.

8.1.2 Biaxial Loading

Biaxial mechanical properties are measured with a pressurized tube (burst) test. The quantities reported refer to the tangential component of stress.

8.1.2.1 Yield Strength

For temperatures from [ ] the design value for biaxial yield strength is:

[

]

For temperatures from [ ] the design value is:

[

]

and for temperatures from [ ] it is:

[

]

[ ] The equations are applicable to cladding.

The design biaxial yield strength for unirradiated $M5_{Framatome}$ material is plotted as a function of temperature in Figure 8-3.

8.1.2.2 Tensile Strength

For temperatures from [ ] the best-estimate value for biaxial tensile strength is:

[ ]

[ ] The best-estimate biaxial tensile strength for unirradiated $M5_{Framatome}$ material is plotted as a function of temperature in Figure 8-4.

8.2 *Tensile Properties of Irradiated Material*

The strength of $M5_{Framatome}$ cladding material increases rapidly under irradiation to a level of saturation that is maintained to high fluences. The irradiated strength is largely saturated within the first year of operation and remains stable for fast fluences up to [ ] $M5_{Framatome}$ cladding material hardness follows a similar increase and saturation early in life. The effects of irradiation on mechanical properties saturate at moderate fluence, so the mechanical properties in the following subsections are applicable for fuel rods [ ]

8.2.1 Uniaxial Loading

8.2.1.1 Yield Strength

The yield strength of irradiated $M5_{Framatome}$ cladding material has been measured under uniaxial stress [ ] The best-estimate uniaxial yield strength is:

[ ]

[

] The equations were developed for cladding and guide tubes with [ ] The best-estimate uniaxial yield strength for irradiated $M5_{Framatome}$ material is plotted as a function of fast fluence in Figure 8-5.

8.2.1.2 Tensile Strength

The tensile strength of irradiated $M5_{Framatome}$ cladding material has been measured under uniaxial stress [ ] The best-estimate uniaxial tensile strength is:

[

]

[

] The equations were developed for cladding and guide tubes with [ ] The best-estimate uniaxial tensile strength for irradiated $M5_{Framatome}$ material is plotted as a function of fast fluence in Figure 8-6.

8.2.2 Biaxial Loading

8.2.2.1 Yield Strength

The yield strength of irradiated $M5_{Framatome}$ cladding material has been measured under biaxial stress [ ] The best-estimate biaxial yield strength is:

[

]

[

] The equations were developed for cladding with [ ] The best-estimate biaxial yield strength for irradiated $M5_{Framatome}$ material is plotted as a function of fast fluence in Figure 8-7.

8.2.2.2 Tensile Strength

The tensile strength of irradiated $M5_{Framatome}$ cladding has been measured under biaxial stress [ ] The best-estimate biaxial tensile strength is:

[

]

[

] The equations were developed for cladding with [ ] The best-estimate biaxial tensile strength for irradiated $M5_{Framatome}$ cladding is plotted as a function of fast fluence in Figure 8-8.

8.3 *Elongation*

The testing that established the yield strength and tensile strength also measured elongation. For tests from [ ] in both uniaxial and biaxial loading, the total elongation of unirradiated $M5_{Framatome}$ cladding is always greater than [ ] With irradiation, the strength increases and the elongation decreases. However, irradiated cladding retains uniform elongation [

] The effects of irradiation on mechanical properties saturate at moderate fluence, so there will not be a significant additional change in elongation [ ]

Figure 8-1: Design Uniaxial Yield Strength of Unirradiated $M5_{Framatome}$ Material as a Function of Temperature

Figure 8-2: Design Uniaxial Tensile Strength of Unirradiated $M5_{Framatome}$ Material as a Function of Temperature

Figure 8-3: Design Biaxial Yield Strength of Unirradiated $M5_{Framatome}$ Material as a Function of Temperature

Figure 8-4: Best-Estimate Biaxial Tensile Strength of Unirradiated $M5_{Framatome}$ Material as a Function of Temperature

Figure 8-5: Best-Estimate Uniaxial Yield strength of Irradiated $M5_{Framatome}$ Material as a Function of Fast Fluence

Figure 8-6: Best-Estimate Uniaxial Tensile Strength of Irradiated $M5_{Framatome}$ Material as a Function of Fast Fluence

Figure 8-7: Best-Estimate Biaxial Yield Strength of Irradiated $M5_{Framatome}$ Material as a Function of Fast Fluence

Figure 8-8: Best-Estimate Biaxial Tensile Strength of Irradiated $M5_{Framatome}$ Cladding as a Function of Fast Fluence

9.0 OXIDATION AND HYDROGEN PICKUP DURING NORMAL OPERATION

This section discusses topics related to oxidation and hydrogen pickup. General corrosion and hydrogen pickup in primary water are discussed in Sections 9.1 and 9.2, respectively. Framatome's corrosion and hydriding databases are discussed in Section 9.3. The morphology and orientation of hydrides in irradiated $M5_{Framatome}$ cladding have implications for mechanical performance of fuel cladding. Section 9.4 demonstrates that hydrides in $M5_{Framatome}$ cladding retain a favorable morphology even at high burnups. Finally, Section 9.5 discusses limits on oxidation and hydrogen concentration.

9.1 *Corrosion Rate*

Corrosion of $M5_{Framatome}$ components includes [

]

[

]

[

]

The $M5_{Framatome}$ material corrosion validation database, Figure 6-4, shows the corrosion of $M5_{Framatome}$ cladding [

]

9.2 *Hydrogen Pickup*

[

]

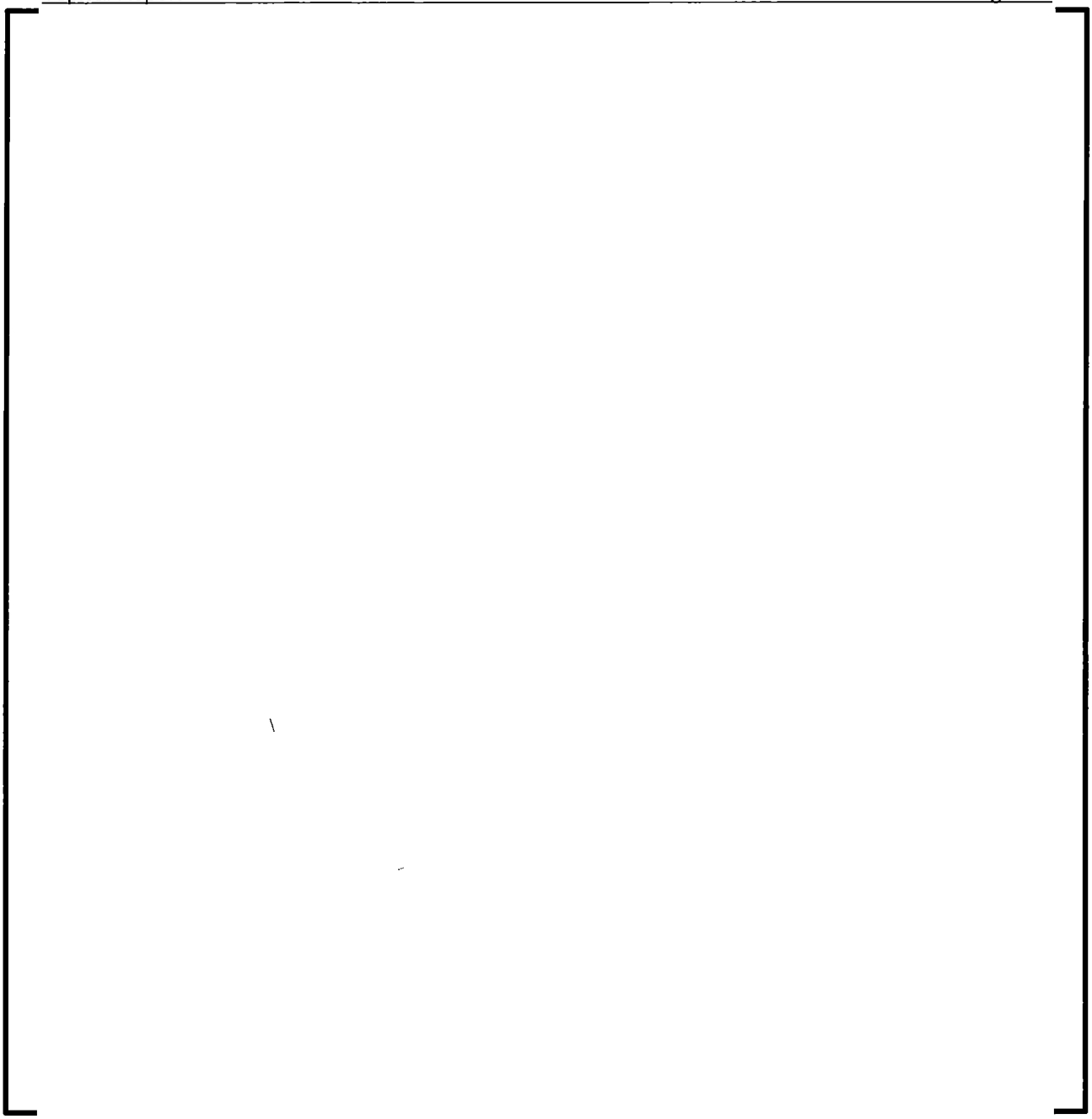

9.3 *Corrosion and Hydriding Databases*

Measurements of corrosion and hydriding of $M5_{Framatome}$ cladding are discussed in Section 4.3.14.2 of Reference [4] and shown in Figure 6-4 and Figure 9-2.

[

[

] A comparison between measured and predicted spacer grid oxide thicknesses is provided in Figure 9-6, and a similar comparison for spacer grid hydrogen concentration is provided in Figure 9-7.

9.4 *Hydride Morphology in Cladding*

As discussed in Section 9.2, $M5_{Framatome}$ components tend to pick up hydrogen as a result of corrosion in a reactor. [

]

This section nevertheless discusses hydrides and demonstrates that they have a limited and well-understood effect on properties. The understanding of hydrides provides assurance that, if hydrides were present, they would not cause unacceptable degradation of performance. The morphology of hydrides in $M5_{Framatome}$ components is described, and the morphology is used to show that the effects of hydride morphology are conservatively bounded by existing regulatory guidance.

Because of the brittleness of zirconium hydride, hydrides tend to reduce ductility in the direction perpendicular to the plane of the hydrides. Radially oriented hydrides are therefore expected to reduce the circumferential ductility of fuel cladding and may reduce the resistance to cladding failure during a transient. In contrast, circumferentially oriented hydrides are expected to have a smaller effect on circumferential ductility.

Hydride morphology has been studied for both unirradiated and irradiated conditions. In the unirradiated condition, samples were either electrolytically charged to a hydrogen concentration of 140 to 220 ppm or charged in hydrogen gas to a concentration of about 200 ppm (Section II.A of Reference [13]). The observed hydrides were predominantly circumferential (Section II.A and Figure 2 of Reference [13]). That result appears to reflect the texture of the cladding and the habit plane for hydrides.

Hydride morphology was also determined for irradiated cladding. In one test, fuel was irradiated in French 900-MW reactors for 5 and 6 annual cycles. The fuel achieved average burnups of 56 to 67 GWd/mtU, and hydrogen concentrations in these samples ranged from 50 to 100 ppm (Section II.A of Reference [13]). The observed hydrides were predominantly circumferential (Section II.A and Figure 3 of Reference [13]).

Typical hydride morphology at room temperature is shown in Figure 9-8.

Because hydrides are brittle, a draft regulatory guide (Reference [14]) discusses the effects of hydrogen on failure by pellet-cladding mechanical interaction (PCMI). The guide states that recrystallized cladding "tends to exhibit randomly oriented zirconium hydride platelets" (Section C.2.3.5 of Reference [14]). [

]

9.5 *Limits on Oxidation and Hydriding*

To ensure that mechanical analyses of fuel assemblies remain conservative, [

]

Hydride limits for $M5_{Framatome}$ cladding are set by the safety criteria affected by hydrogen concentrations. Therefore, no general hydride limit is established.

Table 9-1: Constants for Corrosion of $M5_{Framatome}$ Components

[ ]

Figure 9-1: $M5_{Framatome}$ Cladding Hydrogen Content vs. Burnup (through December 2017)

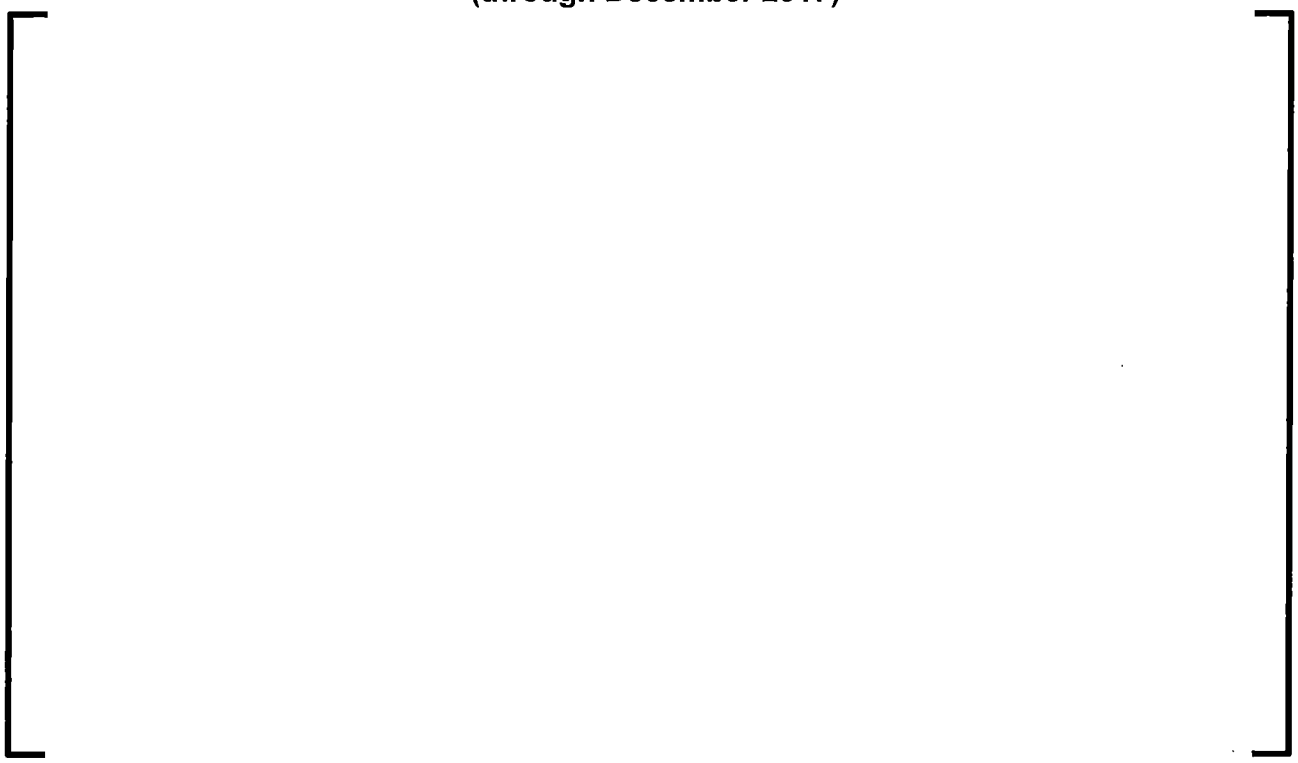

Figure 9-2: Measured and Predicted Hydrogen Concentration for $M5_{Framatome}$ Cladding

Figure 9-3: Post-Transition Hydrogen Pickup Fraction as a Function of Average Oxidation Rate

Figure 9-4: Comparison of Measured and Predicted Oxide Thickness for Guide Tubes

Figure 9-5: Comparison of Measured and Predicted Hydrogen Concentration for Guide Tubes

Figure 9-6: Comparison of Measured and Predicted Oxide Thickness for Spacer Grids

Figure 9-7: Comparison of Measured and Predicted Hydrogen Concentration for Spacer Grids

Figure 9-8: Cladding Hydride Morphology in High Burnup Assembly at Elevations of 645 mm (top) and 2847 mm (bottom)

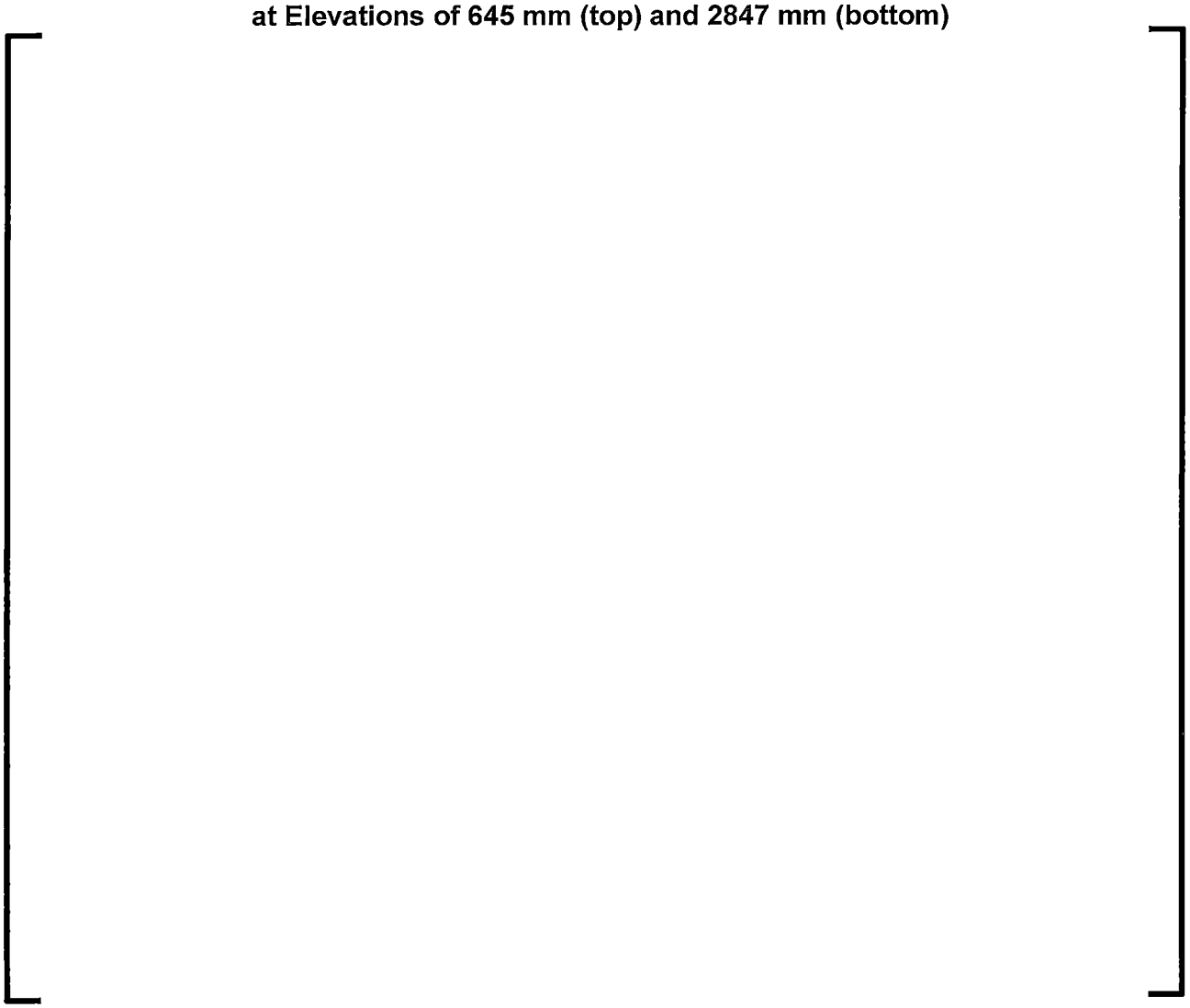

10.0 COMPONENT PERFORMANCE

This section discusses various aspects of performance that are relevant to fuel rod failure. Fuel system performance is evaluated per the requirements of ASME code, Section III, Division 1, subsection NG (Reference [16]). Sections 10.1 and 10.2 provide limits for fuel rod stress and buckling, respectively, and Section 10.3 details the cladding collapse by creep. Transient cladding strain limits are discussed in Section 10.4, and Section 10.5 discusses cladding fatigue resistance. Fretting wear is discussed in Section 10.6.

10.1 *Fuel Rod Stress Limits*

Consistent with NUREG-0800 Section 4.2 (Reference [3]), the design basis for fuel cladding stress is that the fuel system will not be damaged by excessive stresses. The stress limits apply to various mechanisms of fuel rod failure, including Timoshenko buckling, columnar buckling, and mechanical fracturing.

Stress intensity limits for fuel rod stress analysis are derived from the ASME code, Section III, Division 1, subsection NB (Reference [16]). The allowable stress intensity limits for $M5_{Framatome}$ cladding are based on the biaxial strength at operating temperature. Justification for the difference in the stress intensity limits under compressive and tensile conditions for normal operation and AOOs was provided in Section I.2 of Reference [1]. Testing has shown that the failure mode of cladding under compression is buckling, not exceeding yield strength. The testing also shows that the Timoshenko buckling criteria adequately protects against cladding failure. This approach and the use of biaxial strength were approved in Reference [1] and have been used in licensing $M5_{Framatome}$ cladding material in a large number of batch applications.

[

]

The ASME Code Section II, Part D (Reference [18]) is used as a guide for defining the design stress intensity, Sm, as:

[

]

With in-core exposure, the strength of $M5_{Framatome}$ material rapidly increases with [

] Testing has shown the $M5_{Framatome}$ material maintains sufficient ductility in the fully irradiated condition to warrant the use of the ASME code techniques. The definition of the allowable stress intensity discussed herein is based on properties from biaxial tensile tests (burst tests).

The limits for Normal Operations, including AOOs (and Operating Basis Earthquake, if applicable) derived from the ASME Code, Section III, Division 1 (Reference [16], Subsection NB and Appendix XIII) are as follows:

[

]

The limits for faulted conditions (i.e., Safe Shutdown Earthquake and Loss of Coolant Accident) derived from the ASME Code, Section III, Division 1 (Reference [16], Subsection NB and Appendix XIII) for Service Level C loadings are as follows:

[

]

Table 10-1 provides the stress limits in tabular form.

10.2 *Fuel Rod Buckling*

In addition to the stress criteria defined in Section 10.1, the buckling behavior of fuel rods is evaluated. [

]

10.3 *Cladding Creep Collapse*

The cladding creep collapse is determined by using an approved fuel performance code to generate creep collapse initialization conditions and then using the CROV code (Reference [19]) to perform the cladding creep collapse analysis. [

]

10.4 *Transient Cladding Strain*

Mechanical tests and ramp tests have been performed that demonstrate that the 1% strain criterion is conservative for $M5_{Framatome}$ cladding material [

]

10.5 *Fuel Rod Fatigue*

The design criterion for cladding strain fatigue is that the cumulative fatigue usage factor be less than 0.9 using the O'Donnell and Langer fatigue curve, which includes a minimum safety factor of 2 on the stress amplitude or a minimum safety factor of 20 on the number of cycles, whichever is more conservative. The cladding fatigue evaluation is based on the cyclic stress amplitudes calculated for the specified number of duty cycles during the irradiation life. Procedures for the fatigue analysis follow those outlined in the ASME Boiler and Pressure Vessel Code (Reference [18]). To determine the total fatigue usage factor of the cladding, all possible Condition I and II events are considered. [

]

The criterion was shown to be conservative for $M5_{Framatome}$ material in accordance with Reference [1] based on $M5_{Framatome}$ material cyclic strain fatigue tests.

10.6 *Fretting*

Framatome's design criterion for fretting wear (i.e., fuel rod failures due to fretting shall not occur) remains the same as that previously approved by the NRC per References [8], [20], and [21]. The fretting wear criterion remains applicable [

]

Fuel rod fretting wear depends largely on design features of the spacer grid and fuel rod retention system and on the hydraulic environment in which the fuel rod operates (References [1] and [8]). No adverse fretting wear has been attributed to $M5_{Framatome}$ cladding, as shown by extensive out-of-core design validation testing and in-reactor experience, including [ ]

Framatome's standard method of design validation for fretting wear is a 1000-hour life and wear test in concert with in-reactor operating experience of LTAs and batch fuel. This method has been approved by the NRC per References [1], [8], [20], [21], and [22]. Life and wear testing utilizes a full scale fuel assembly representing EOL rod-spacer grid support conditions. Tests are run for 1000 hours in water at simulated operating conditions (temperature, pressure, and flow). These tests determine the fretting wear characteristics at the grid-to-rod interfaces.

Framatome's extensive operating experience with $M5_{Framatome}$ components is described in Section 6.0. [ ] Review of $M5_{Framatome}$ cladding failures shows no fretting-related failures in any fuel assemblies with average burnups greater than [ ] No influence of [ ] on $M5_{Framatome}$ cladding material has been observed for fretting-related failures. $M5_{Framatome}$ cladding material has not been found to be more susceptible to fretting-related failures than other zirconium alloys.

In addition to the extensive out-of-core test and in-reactor experience, the $M5_{Framatome}$ material attributes under irradiation related to fretting performance remain applicable [ ] The hardness as correlated with yield strength (Section 8.2), cladding oxidation (Section 9.1), the corresponding hydrogen pickup (Section 9.2), and creep (Section 11.1) are shown to be consistent and stable for $M5_{Framatome}$ cladding [ ]

Table 10-1: Stress Limits for $M5_{Framatome}$ Cladding

[ ]

11.0 GROWTH AND CREEP

11.1 *Irradiation Induced Free Growth and Creep*

$M5_{Framatome}$ cladding is modeled in terms of irradiation creep, thermal creep, plasticity, and free growth. Free growth is a permanent strain dependent on fast neutron fluence and temperature. The free growth models are described in the fuel rod performance codes (e.g., Reference [4]).

The contribution of irradiation induced free growth to cladding elongation is limited. Fuel rod elongation is mainly determined by cladding creep-down anisotropy before pellet-cladding contact and by pellet-cladding axial interaction after contact.

Creep results from stress on a component. The irradiation creep and thermal creep in normal reactor conditions are modeled in a "low stress" creep law, whereas the "high stress" creep law models the viscoplasticity at high stresses. The creep models are described in the fuel rod performance codes (e.g., Reference [4]). For mechanical design purposes, fuel assembly and fuel rod growth are calculated with other models.

The low stress model is representative of normal in-reactor conditions under which fretting wear may occur. Irradiation creep is a major contributor to the total diametral strain of the cladding, which can affect the fuel rod-spacer grid support condition. [

]

11.2 *Fuel Rod Axial Growth*

The design basis for fuel rod axial growth is that adequate clearance be maintained between the fuel rod ends and top and bottom nozzles to accommodate the difference in the axial growth of fuel rods and fuel assembly. The clearance between the fuel rod top ends and the top nozzle is known as the shoulder gap.

[

]

The validity range extends to a [

]

The fuel rod axial growth model prediction as a function of [

] in Figure 11-1 shows that the model remains conservative. The complete operating experience is plotted as fuel rod axial growth versus [

] in Figure 6-3. Figure 11-2 represents the upper bound model as a function of [

]

11.3 *Fuel Assembly Growth*

The fuel assembly growth shall not exceed the minimum clearance between the fuel assembly and the upper plate in the reactor. The upper and lower $M5_{Framatome}$ fuel assembly design growth limits generically approved in Section 6.1.7.2 of Reference [8] remain applicable and are defined in terms [ ]:

[ ]

Figure 11-3 provides the $M5_{Framatome}$ [ ] growth design limits and corresponding data, [ ] The fuel assembly growth upper and lower design limits are for generic application [ ] using $M5_{Framatome}$ guide tubes.

11.4 *Fuel Rod Bowing*

Fuel rod bow is driven by the irradiation growth of the fuel rods and friction with the supporting guide structure. $M5_{Framatome}$ fuel rods are expected to have rod bow within the envelope established for Zircaloy-4 fuel rods in Reference [15]. The effects of bowing are included in the departure from nucleate boiling (DNB) analysis by a DNB ratio penalty when rod bow is greater than a predetermined amount. This methodology for rod bow is consistent with Reference [3].

The approved performance and penalties established in References [15], [23], and [24] apply to the $M5_{Framatome}$ cladding designs.

Figure 11-1: Predicted Fuel Rod Axial Growth by the Upper Bound Model as a Function of Experimental Axial Growth from AFA, GAIA, and HTP Fuel Assemblies

Figure 11-2: Fuel Rod Axial Growth Operating Experience as a Function of Fuel Rod Average Burnup for GAIA and HTP Fuel Assemblies Compared to the Fuel Rod Axial Growth Upper Bound (UB) Model

Figure 11-3: $M5_{Framatome}$ HTP Fuel Assembly Growth

12.0 MATERIAL PERFORMANCE IN NON-LOCA

Non-LOCA events are evaluated for various initiating events resulting in a range of plant and core responses. Non-LOCA events address several acceptance criteria including those associated with the fuel (i.e., SAFDLs) as well as plant system-related limits (e.g., system overpressure). Methodologies for non-LOCA analyses are defined and approved elsewhere. $M5_{Framatome}$ cladding properties and models approved for use in the current non-LOCA methodologies were reviewed and found to be appropriate for continued use in those methods. Updates to $M5_{Framatome}$ cladding properties or models in this report do not invalidate those models approved for use in previously defined non-LOCA methodologies.

13.0 MATERIAL PERFORMANCE IN LOCA

In addition to generic properties and models, there are models necessary to describe the performance of $M5_{Framatome}$ cladding during a LOCA event. These include high temperature oxidation and clad swelling and rupture. These models are applied in the Framatome LOCA methods in various ways, but the base models themselves are the same. Furthermore, the failure of the cladding during a LOCA can depend on material-specific behavior, and the limits used in the analyses therefore must be assessed.

13.1 *Swelling and Rupture*

Cladding swelling and rupture at high temperatures is a phenomenon encountered during LOCA events. Cladding swelling and rupture behavior is variable depending on the cladding material type. This section provides the swelling and rupture model for the $M5_{Framatome}$ cladding material.

13.1.1 Swelling and Rupture Model Background

A distinct swelling and rupture model is required since $M5_{Framatome}$ cladding has different swelling and rupture behavior than Zircaloy, which uses the NUREG-0630 model (Reference [25]). [

] The NRC-approved swelling and rupture model is found in Appendix K of Reference [1].

13.1.2 Swelling and Rupture Database Updates

Following NRC approval of the swelling and rupture model in Appendix K of Reference [1], EDGAR testing of $M5_{Framatome}$ cladding continued. [

]

Three LOCA methods utilize the swelling and rupture model approved in Reference [1]. Reference [1] directly addressed the incorporation of the $M5_{Framatome}$ cladding properties into the B&W LOCA methodology (Reference [26], as amended by Reference [27]) through user inputs. The $M5_{Framatome}$ material properties in the W&CE plant type Small Break LOCA methodology (Reference [28]) were incorporated by Reference [8]. The Realistic Large Break LOCA (RLBLOCA) Revision 0 methodology (Reference [29]) did not include the swelling and rupture model. The swelling and rupture model is part of the RLBLOCA Revision 3 methodology (Reference [10]).

The approval of Revision 2 of this topical report updates the approved swelling and rupture model to be used in those methodologies that incorporate the model, including the following:

[

]

13.1.3 Description of EDGAR Tests

[

]

13.1.4 Swelling and Rupture Model

The swelling and rupture model was developed in a similar manner to the NUREG-0630 (Reference [25]) Zircaloy models, and accordingly has the same general features.

[

]

[

]

13.1.4.1 Rupture Temperature

The rupture temperature [

] Additionally, occurrence of rupture affects downstream calculations, such as cladding oxidation.

The NRC-approved rupture temperature correlation and its development are described in Section K.5 of Reference [1]. No subsequent modifications to the rupture temperature correlation were required due to the additional EDGAR data mentioned previously (Section 13.1.2). The approved rupture temperature correlation is provided below.

[ ]

13.1.4.2 Pre-Rupture Strain

[ ]

13.1.4.2.1 Treatment Prior to Rupture

[
]

13.1.4.2.2 Treatment At and After Rupture

Practically, when rupture occurs, swelling ceases and the cladding is permanently deformed by the degree of pre-rupture strain at the time of rupture. [

]

13.1.4.3 Rupture Strain

During a high-temperature transient, the part of the fuel rod cladding subjected to especially detrimental conditions may begin to swell faster than regions around it, ballooning and ultimately rupturing. Deformation (rupture strain) at the location of rupture depends on temperature, differential pressure (hoop stress), ramp rate, and several other variables such as local temperature variations and metallurgical conditions. The degree of strain at the rupture location affects not only the degree of assembly blockage, but also important LOCA results such as oxidation, hydrogen generation, and cladding temperature.

[

]

[

]

13.1.4.4 Assembly Blockage Factors

It is important to characterize assembly blockage so that effects of clad swelling, such as flow diversion, can be simulated. [

]

[

]

13.2 *High Temperature Steam Oxidation*

LOCA analyses can predict an excursion in cladding temperature in which the reaction of the zirconium-based cladding with the steam environment may become appreciable. The metal-water reaction results in energy release, hydrogen generation, and oxidation of the cladding. This LOCA-associated oxidation process is referred to as high temperature steam oxidation to differentiate it from the cladding oxidation due to normal operation corrosion. To demonstrate the acceptability of the emergency core cooling systems (ECCS) design and compliance with the U.S. NRC criteria specified in 10 CFR 50.46, each consequence of the metal-water reaction must be considered in the LOCA analysis. Appendix K of 10 CFR Part 50 defined specific requirements for LOCA evaluation models and prescribed that the reaction be calculated using the Baker-Just correlation. Oxidation kinetics studies on a variety of zirconium alloys conducted since the initial establishment of 10 CFR 50.46 have demonstrated that the Baker-Just correlation overpredicts the weight gain and zirconium consumed. Chapter 6.13 of NUREG-1230, "Compendium of ECCS Research for Realistic LOCA Analysis," as well as Regulatory Guide (RG) 1.157, "Best-Estimate Calculations of Emergency Core Cooling Performance," recommend the use of the Cathcart-Pawel correlation in realistic evaluation models as allowed by the 1988 revision to 10 CFR 50.46.

Appendix D and additional RAI responses in Appendix I of Reference [1] provided the $M5_{Framatome}$ test data available at the time of the topical submittal and compared the results to the Baker-Just correlation. It was concluded that the kinetics of $M5_{Framatome}$ cladding are similar to those of Zr-4 and that the Baker-Just correlation is acceptable for the conservative calculation of high temperature steam oxidation with $M5_{Framatome}$ cladding. This section presents further test data to confirm the previous conclusion and evaluates the Cathcart-Pawel correlation for best-estimate calculations.

A large number of tests have been performed on $M5_{Framatome}$ and Zr-4 cladding materials as part of the DEZIROX testing program to characterize the cladding performance under high temperature oxidation and post-quench mechanical properties. DEZIROX is a CEA facility with a vertical resistive furnace capable of heating specimens up to 1250 °C. [

]

Figure 13-8 provides a demonstration of the oxidation kinetics at 1200 °C (~2200 °F). The figure includes the ECR converted from the measured weight gain for both $M5_{Framatome}$ and Zr-4 cladding samples and the calculated ECR based on the Baker-Just and Cathcart-Pawel correlations. Figure 13-9 and Figure 13-10 provide the same information but for 1000 °C and 1100 °C, respectively. Figure 13-11 plots the same data at 1250 °C, above the 10 CFR 50.46 PCT limit (1200 °C/ 2200 °F). [

] All four temperature plots demonstrate the expected performance of $M5_{Framatome}$ cladding in relation to the correlations. The Baker-Just correlation is significantly bounding, while the Cathcart-Pawel correlation, for use with realistic methodologies, follows the data trend more closely.

In conclusion, the Appendix K Baker-Just correlation and RG 1.157 Best-Estimate Cathcart-Pawel correlation are acceptable for calculating the metal-water reaction for $M5_{Framatome}$ cladding within the respective evaluation model types.

13.3 *Analytical Limits - 10 CFR 50.46*

10 CFR 50.46 provides the U.S. NRC acceptance criteria for ECCS for light-water nuclear power reactors. Analyses are performed with NRC-approved evaluation models to demonstrate that calculated ECCS cooling performance following postulated LOCAs conforms to the criteria set forth in paragraph (b) of 50.46. The current regulation is only explicitly applicable to "uranium oxide pellets within cylindrical zircaloy or ZIRLO™ cladding". This section addresses the applicability of the regulatory criteria for $M5_{Framatome}$ cladding.

Briefly, 10 CFR 50.46 limits the calculated results such that:

1. The Peak Cladding Temperature (PCT) is less than 2200 °F - This limit is associated with cladding embrittlement and its applicability to $M5_{Framatome}$ cladding will be addressed in this section.

2. The total Maximum Local Oxidation (MLO) is less than 17 percent of the total cladding thickness - This limit is associated with cladding embrittlement and its applicability to $M5_{Framatome}$ cladding will be addressed in this section.

3. The maximum hydrogen generation is less than 1% of the hypothetical amount that would be generated if all of the metal in the cladding cylinders reacted - This limit was imposed to prevent the accumulation of a combustible amount of hydrogen within the reactor building. While the calculation of the hydrogen generated during a LOCA can be dependent on the cladding, the criterion itself is not related to nor affected by the cladding material. This 10 CFR 50.46 criterion is therefore applicable to fuel with $M5_{Framatome}$ cladding.

4. The core geometry remains amenable to cooling - The implication of this criterion is that the core shall remain in a condition that can be readily cooled by the type of short- and long-term cooling mechanisms provided by the plant ECCS. While the calculated core geometry can be dependent on the cladding, the criterion itself is not related to nor affected by the cladding material. This 10 CFR 50.46 criterion is therefore applicable to fuel with $M5_{Framatome}$ cladding.

5. Long-term core cooling is maintained - Maintaining long-term ECCS recirculation coolant delivery provides assurance that core geometry remains stable and further fuel cladding damage (beyond that experienced during the initial period of accident) would be minimal. This is a plant system requirement and the criterion itself is not related to nor affected by the cladding material. This 10 CFR 50.46 criterion is therefore applicable to fuel with $M5_{Framatome}$ cladding.

The high temperature metal-water reaction results in oxidation of the cladding (Section 13.2). The oxidation results in the development of an outer surface Zr-oxide layer and diffusion of oxygen in solid solution into the metal substrate, forming an oxygen-stabilized α-Zr layer, and a β-Zr layer with low oxygen content. With increasing time, diffusion of oxygen into the metal will convert more and more of the beta phase to the oxygen-stabilized alpha phase– the alpha layer grows and the beta region shrinks. Following quench, three distinct regions remain, as shown in Figure 13-12 (Reference [30]), the ZrO_2 layer, the oxygen stabilized alpha layer, and the prior-beta layer. The ZrO_2 layer and oxygen stabilized alpha phase are brittle at low temperature and therefore do not contribute to the cladding integrity. The prior-beta phase ductility and mechanical resistance depend on the oxygen concentration. With sufficiently low oxygen concentrations, the prior-beta region can remain ductile.

When the U.S. LOCA criteria were established in the 1970s, the retention of ductility was considered the best guarantee against potential fragmentation under various types of loading (e.g., thermal-shock, bundle constraint, hydraulic, handling, and seismic forces). The preservation of cladding ductility, via compliance with regulatory criteria on peak cladding temperature ((b)(1)) and local cladding oxidation ((b)(2)), provides a level of assurance that fuel cladding will not experience gross failure and ensures that a coolable core geometry will be maintained. The two criteria are interdependent because the kinetics of the oxidation and embrittlement of the beta layer (e.g. solubility of oxygen) depend on both time and temperature.

The PCT criterion, (b)(1), and total oxidation criterion, (b)(2), were deduced largely from Ring Compression Tests (RCT) performed by Hobson on oxidized Zr-4 cladding samples. After the test, the broken pieces of the ring were reassembled to determine the degree of brittleness. Zero ductility was defined on the basis of the macroscopic geometry of the broken pieces and the morphology of the fracture surface on microscopic scale. The (b)(1) PCT value is essentially an upper limit on the testing database, related to the potential for faster reaction kinetics and greater oxygen solubility in the beta phase. The (b)(2) criterion is the value calculated using the time-and-temperature dependent Baker-Just correlation. Total oxidation is defined in the (b)(2) criterion as:

> the total thickness of cladding metal that would be locally converted to oxide if all the oxygen absorbed by and reacted with the cladding locally were converted to stoichiometric zirconium dioxide.

Thus, the limit value in (b)(2) is a percent Equivalent Clad Reacted, (% ECR). It acts as a surrogate to an explicit material property that can easily be utilized in LOCA accident analyses to ensure cladding survival when taken in concert with the PCT limit.

Mechanical tests were performed on samples oxidized at high temperatures (Section 13.2) to study the post-quench performance of $M5_{Framatome}$ cladding. [

]

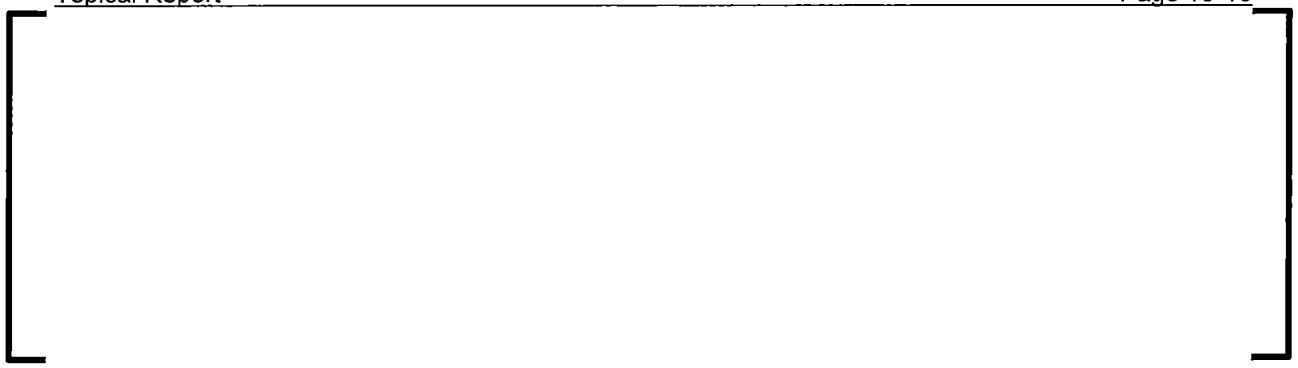

The results of the RCT tests on samples oxidized at 1200 °C are shown in Figure 13-13. The residual ductility is shown as a function of the calculated Baker-Just ECR (% BJ ECR). [

]

[

]

These RCT results demonstrate the comparable performance of Zr-4 and $M5_{Framatome}$ cladding and clearly show that $M5_{Framatome}$ samples were not brittle below the 17% BJ ECR limit (13% CP ECR). This conclusion is further strengthened by Figure 13-14 which presents the same information, but for all four oxidation temperatures. These results are also in line with the results in Reference [30], summarized by Figure 24, and the proposed NRC-acceptable PQD limit in Figure 2 of Reference [31] that show that unirradiated $M5_{Framatome}$ cladding retains ductility to at least 18% CP ECR and 2200 °F.

Section 13.2 demonstrated that there is no increase in the oxidation kinetics as compared to Zr-4 below 1250 °C (2282 °F) and that the Baker-Just correlation is applicable. In combination with the RCT results demonstrated in this section, it is concluded that the 2200 °F and 17% ECR limit are applicable to $M5_{Framatome}$ cladding.

Table 13-1: Slow and Fast Ramp Rate Pre-Rupture Strain Model for $M5_{Framatome}$ Cladding

Table 13-2: Slow and Fast Ramp Rate Rupture Strain Model for $M5_{Framatome}$ Cladding

Table 13-3: Slow and Fast Ramp Rate Assembly Blockage Model with $M5_{Framatome}$ Cladding

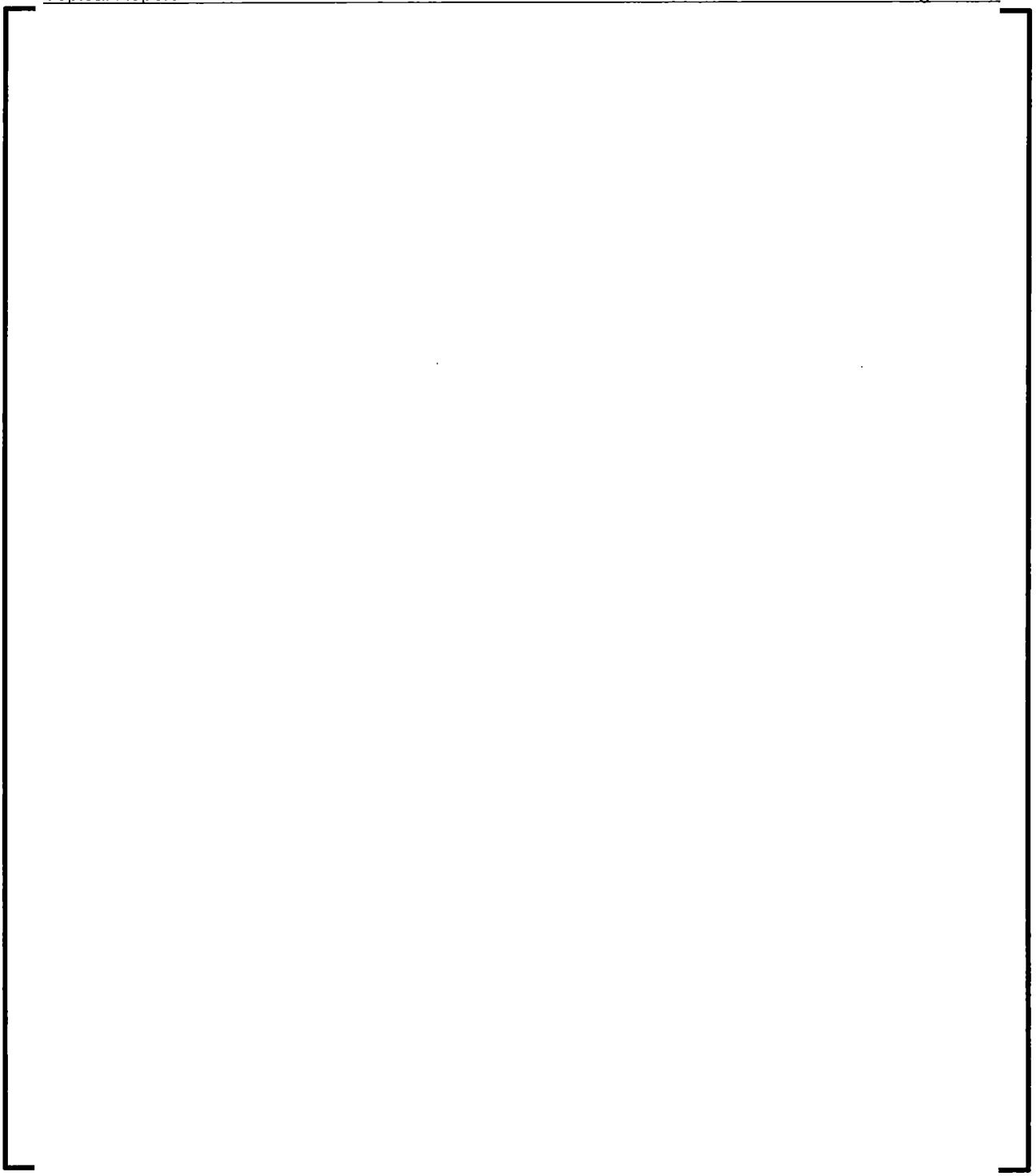

Figure 13-1: EDGAR Test Apparatus

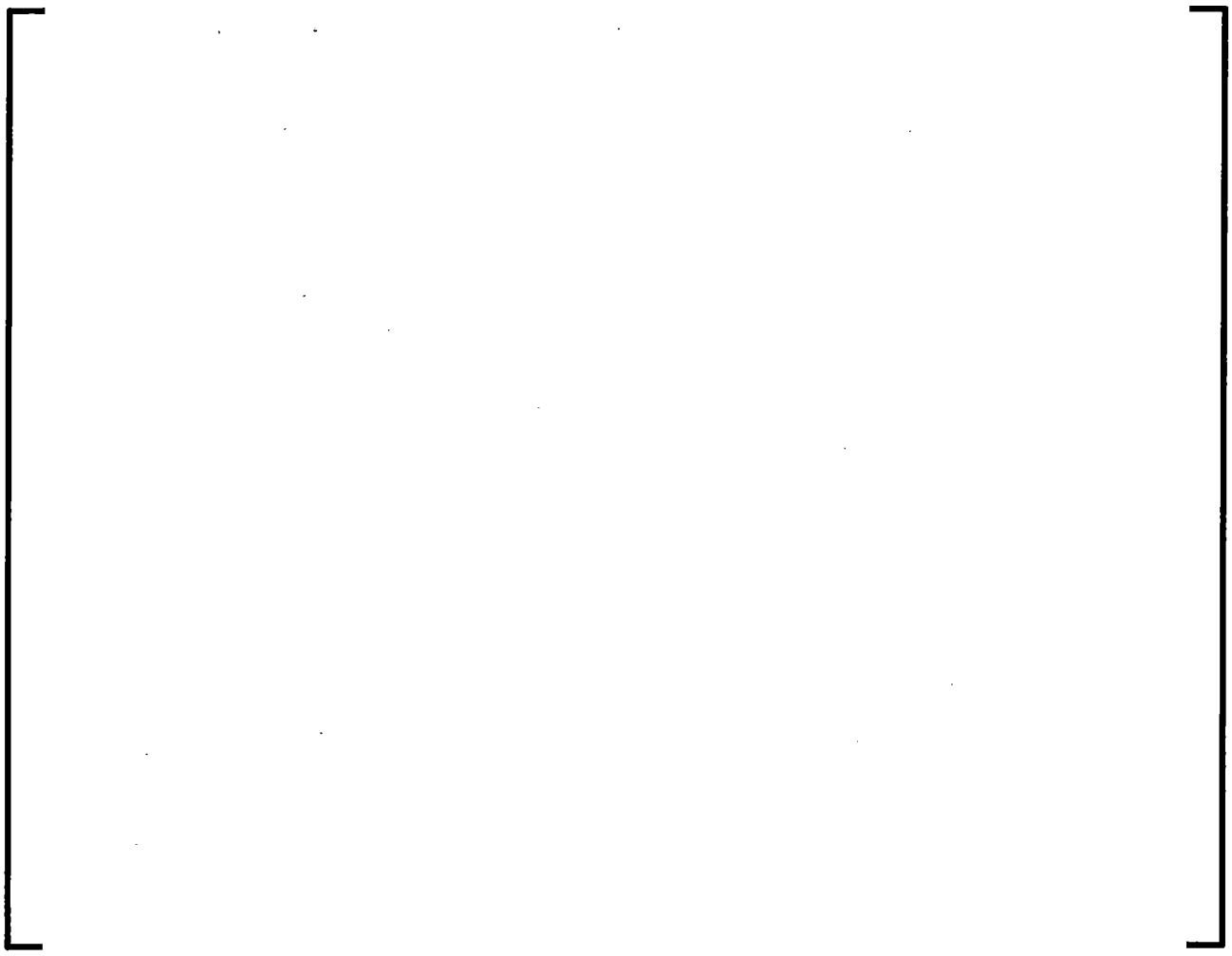

Figure 13-2: Ruptured Cladding Sample Schematic

Figure 13-3: Slow and Fast Heating Ramp Rate Pre-Rupture Strain Curves for $M5_{Framatome}$ Cladding

Figure 13-4: Fast Heating Ramp Rate Rupture Strain Curves and EDGAR Rupture Strain Data for $M5_{Framatome}$ Cladding

Figure 13-5: Slow and Fast Heating Ramp Rate Rupture Strain Curves for $M5_{Framatome}$ Cladding

Figure 13-6: Fast Heating Ramp Rate Assembly Blockage Curves with $M5_{Framatome}$ Cladding

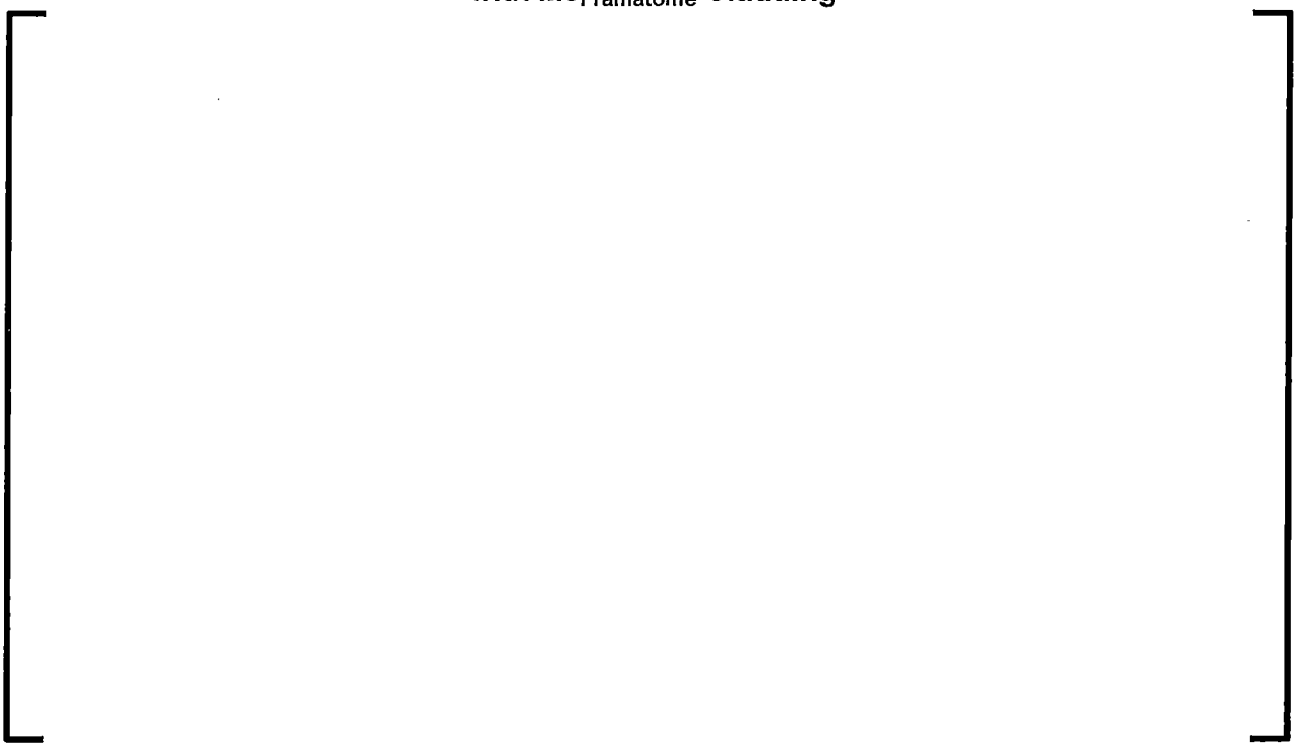

Figure 13-7: Slow and Fast Heating Ramp Rate Assembly Blockage Curves with $M5_{Framatome}$ Cladding

Figure 13-8: Measured and Calculated % ECR at 1200 °C

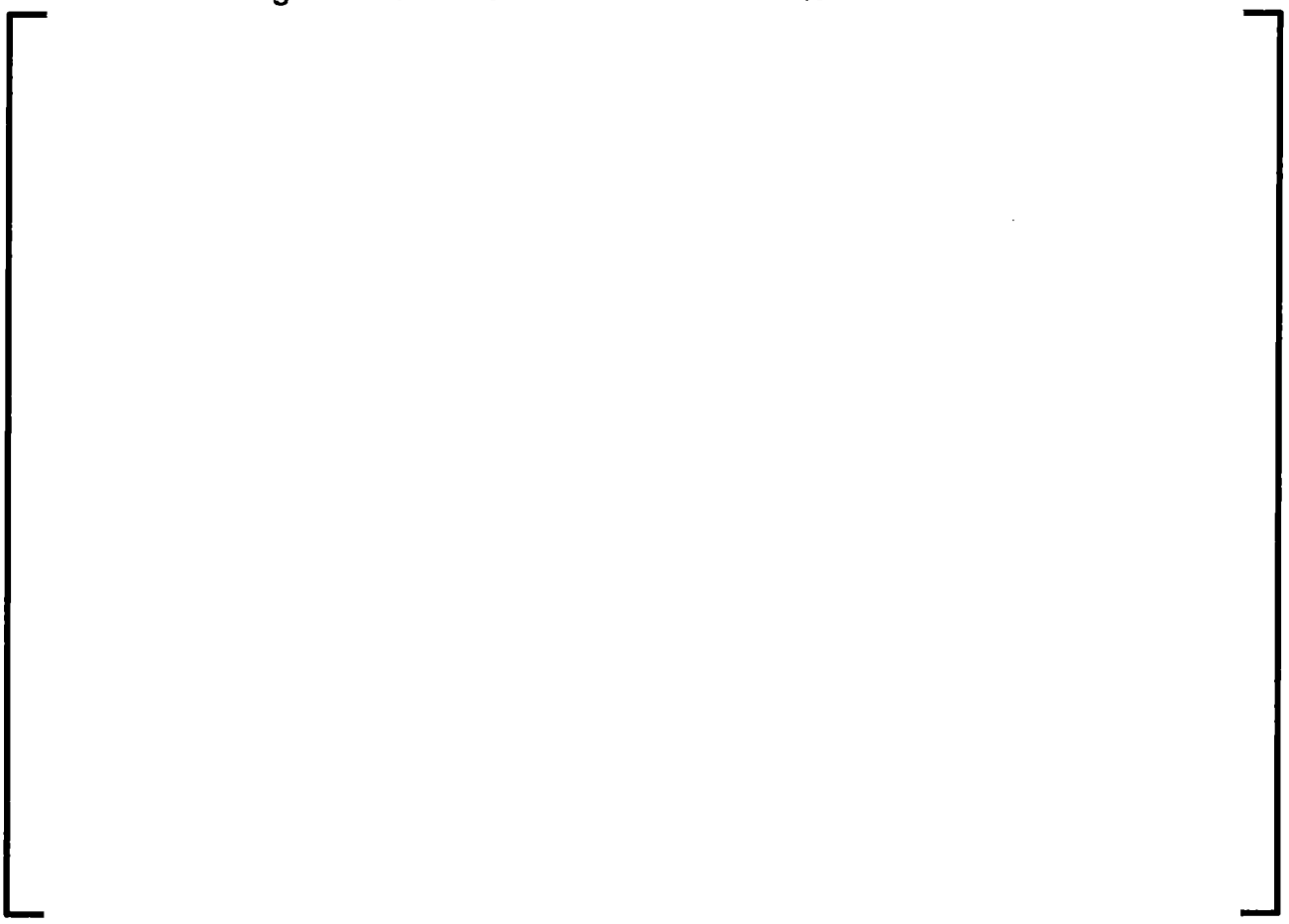

Figure 13-9: Measured and Calculated % ECR at 1000 °C

Figure 13-10: Measured and Calculated % ECR at 1100 °C

Figure 13-11: Measured and Calculated % ECR at 1250 °C

Figure 13-12: Qualitative Diagram of Oxygen Concentration in Zircaloy Cladding Exposed at High Temperature to Steam on the Outside Surface and Cooled to Room Temperature

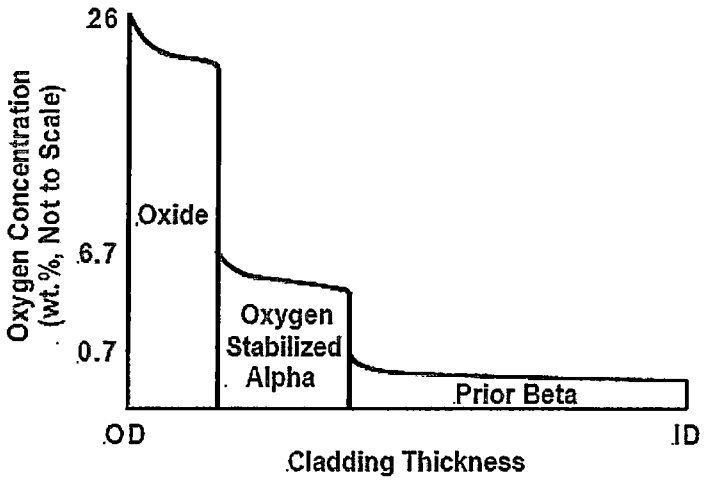

Figure 13-13: RCT Residual Ductility vs. Calculated ECR, 1200 °C Oxidation

Figure 13-14: RCT Residual Ductility vs. Calculated ECR, 1000 °C - 1250 °C Oxidation

14.0 SURVEILLANCE

Framatome monitors the performance of $M5_{Framatome}$ components in commercial reactors worldwide. PIE of $M5_{Framatome}$ fuel assembly components are performed at poolside or in a hot cell and the data are evaluated against Framatome's databases and performance models. Once the data are validated, they are added to the databases. Framatome's U.S. PIE plans are established [ ] and ensure material and component performance are monitored.

Framatome intends to continue the established process for PIE planning and surveillance of fuel performance. As fuel rod average burnup limits are increased, surveillance will be focused on PIE of end-of-life fuel assemblies to confirm expected behavior and applicability of models to higher fuel rod average burnups.

15.0 UPDATE PROCESS

Framatome plans to continue to monitor the performance of $M5_{Framatome}$ components. Through various material test programs, Framatome also plans to continue to gather in-core, out-of-core, and test reactor data on $M5_{Framatome}$ components. Data may be obtained for high [ ] for new designs, or outside the range of applicability of current models. As a result, it may be desirable to adjust the models or update their applicability ranges presented in this report. These activities allow Framatome to continuously expand its knowledge and improve its predictive performance tools for $M5_{Framatome}$ components.

15.1 *Model Updates*

As $M5_{Framatome}$ material data are obtained the Framatome PIE database will be expanded. Periodically, the models and applicability ranges discussed in Sections 7.0 to 13.0 will be reviewed against the growing database. If the data support a modification to any of the $M5_{Framatome}$ material models used for design analyses, updated models will be derived following the same process used to fit the original models to the data. Model forms presented in this topical report will be maintained. If any $M5_{Framatome}$ material models are updated, the internal Framatome design change process will be followed. This change process includes documentation and justification of the update and evaluation of the impact on future design analyses. Any updates to the models presented in Sections 7.0 to 13.0 will be documented in internal Framatome documents.

15.2 *Updates to Applicability Ranges*

Applicability ranges are established generically for $M5_{Framatome}$ components in Section 4.0. Sections on individual models provide more specific applicability ranges, such as for temperature. When data are obtained outside of the approved applicability ranges, extension of the approved models to that range will be evaluated. If the extension fits the measured data, the applicability range of that model may be extended to cover the evaluated data. If the extension does not fit the data, then one of the following actions will be taken:

- The applicability range will not be extended, and the current approved model and applicability range will be maintained, or
- The model will be updated per Section 15.1 to cover the dataset with an extended applicability range.

15.3 *NRC Notifications*

A summary of any updates made to the models will be provided to the NRC in a letter report for information.

The update process ensures that design margins are maintained and updates are examined with regard to the limitations specified in the NRC's Safety Evaluation. If the model updates are outside of the NRC's Safety Evaluation limitations, then one of the following actions will be taken:

- No credit taken for the update
- Update documented for NRC review and approval
- Update included in a License Amendment Request for site-specific approval.

16.0 REFERENCES

[1] BAW-10227P-A Revision 1, "Evaluation of Advanced Cladding and Structural Material (M5) in PWR Reactor Fuel," June 2003.

[2] BAW-10227 Revision 1 Supp. 1P-A Revision 0, "Evaluation of Advanced Cladding and Structural Material (M5) in PWR Reactor Fuel," June 2019.

[3] NUREG-0800 Revision 3, "Section 4.2, Fuel System Design," in Standard Review Plan, March 2007.

[4] ANP-10323P Revision 1, "GALILEO Fuel Rod Thermal-Mechanical Methodology for Pressurized Water Reactors," June 2018.

[5] D. L. Douglass, "The Metallurgy of Zirconium," Atomic Energy Review, Supplement, 1971.

[6] G. E. Dieter Jr., Mechanical Metallurgy, New York: McGraw-Hill Book Company, Inc., 1961.

[7] ANP-10334P-A Revision 0, "Q12™ Structural Material," September 2017.

[8] BAW-10240P-A Revision 0, "Incorporation of M5™ Properties in Framatome ANP Approved Methods," May 2004.

[9] R. W. Powell and R. P. Tye, "The thermal and electrical conductivities of zirconium and of some zirconium alloys," Journal of The Less Common Metals, vol. 3, pp. 202-215, 1961.

[10] EMF-2103P-A Revision 3, "Realistic Large Break LOCA Methodology for Pressurized Water Reactors," June 2016.

[11] W. D. Biggs, The Mechanical Behaviour of Engineering Materials, Oxford, UK: Pergamon Press, 1965.

[12] American Society of Mechanical Engineers, "Section II, Part D, Properties (Customary)," in Boiler and Pressure Vessel Code, New York, New York, American Society of Mechanical Engineers, 2019 Edition.

[13] ANP-10285Q8P Revision 0, "Response to Sixth Request for Additional Information – ANP-10285P "U.S. EPR Fuel Assembly Mechanical Design Topical Report" RAI 60, 61, 62 and 63," January 2011.

[14] P. Bouffioux, A. Ambard, A. Miquet, C. Cappelaere, Q. Auzoux, M. Bono, O. Rabouille, S. Allegre, V. Chabretout and C. P. Scott, "Hydride Reorientation in M5® Cladding and Its Impact on Mechanical Properties," in LWR Fuel Performance Meeting, Top Fuel 2013, Charlotte, NC, USA, September 15-19, 2013.

[15] DG-1327 (U.S. NRC ADAMS accession number ML16124A200), "Pressurized Water Reactor Control Rod Ejection and Boiling Water Reactor Control Rod Drop Accidents".

[16] BAW-10186P-A Revision 2, "Extended Burnup Evaluation," June 2003.

[17] American Society of Mechanical Engineers, "Section III, Rules for Construction of Nuclear Facility Components," in Boiler and Pressure Vessel Code, New York, New York, American Society of Mechanical Engineers, 2019 Edition.

[18] ANP-10337P-A Revision 0, "PWR Fuel Assembly Structural Response to Externally Applied Dynamic Excitations," April 2018.

[19] BAW-10084P-A, Revision 3.0, "Program to determine in-reactor performance of BWFC fuel cladding creep collapse".

[20] EMF-92-116(P)(A) Revision 0, "Generic Mechanical Design Criteria for PWR Fuel Designs," February 1999.

[21] ANP-10342PA, Revision 0, GAIA Fuel Assembly Mechanical Design, September 2019.

[22] BAW-10179P-A Revision 3, "Safety Criteria and Methodology for Acceptable Cycle Reload Analyses," October 1999.

[23] BAW-10179P-A Revision 9, "Safety Criteria and Methodology for Acceptable Cycle Reload Analyses," November 2017.

[24] XN-75-32(P)(A) Supplements 1, 2, 3, and 4, "Computational Procedure for Evaluating Fuel Rod Bowing," October 1983.

[25] D.A. Powers and R.O. Meyer, NUREG-0630, "Cladding Swelling and Rupture Models for LOCA Analysis," April 1980.

[26] BAW-10192P-A Revision 0, "BWNT LOCA – BWNT Loss-of-Coolant Accident Evaluation Model for Once-Through Steam Generator Plants," June 1998.

[27] BAW-10192P-A Revision 0 Supplement 1P-A Revision 0, "BWNT LOCA – BWNT Loss-of-Coolant Accident Evaluation Model for Once-Through Stream Generator Plants," November 2017.

[28] EMF-2328(P)(A) Revision 0, "PWR Small Break LOCA Evaluation Model, S-RELAP5 Based," March 2001.

[29] EMF-2103(P)(A) Revision 0, "Realistic Large Break LOCA Methodology for Pressurized Water Reactors," April 2003.

[30] NUREG/CR-7219, "Cladding Behavior During Postulated Loss-of-Coolant Accidents," NRC ADAMS Accession Number ML16211A004, July 2016.

[31] Pre-Decisional Regulatory Guide 1.224, "Establishing Analytical Limits for Zirconium-Alloy Cladding Material," NRC ADAMS Accession Number ML16005A133.

[32] BAW-10164P-A Revision 6, "RELAP5/MOD2-B&W – An Advanced Computer Program for Light Water Reactor LOCA and Non-LOCA Transient Analysis," June 2007.